A simplified isotope dilution approach for the U-Pb dating of speleogenic and other low-^{232}Th carbonates by multi-collector ICP-MS

Andrew J. Mason[1], Anton Vaks[1,a], Sebastian F. M. Breitenbach[b], John N. Hooker[1,b], Gideon M. Henderson[1]

[1]Department of Earth Sciences, University of Oxford, South Parks Road, Oxford, OX1 3AN, United Kingdom.
[2]Department of Geography and Environmental Sciences, Northumbria University, Ellison Place, Newcastle upon Tyne, NE1 8ST, United Kingdom.
[a]Present address: Geological Survey of Israel, 32 Yeshayahu Leibowitz Street, 9692100 Jerusalem, Israel.
[b]Present address: Department of Geosciences, Penn State University, 503 Deike Building, University Park, PA 16802, USA.

Correspondence to: Andrew J. Mason (Andrew.Mason@earth.ox.ac.uk)

Abstract. We describe a new method for the measurement of U/Pb ratios by isotope dilution multi-collector inductively coupled plasma mass spectrometry (MC-ICP-MS) for the dating of geologically young clean carbonates, particularly speleothems. The method is intended for materials containing little or no initial ^{232}Th. We illustrate and validate the method with four examples ranging from 0.57 Ma to 20 Ma old. The new method is capable of applying the ^{235}U-^{207}Pb and ^{238}U-^{234}U-^{206}Pb chronometers, common Pb and quantifiable residual ^{234}U/^{238}U disequilibrium permitting. These provide an alternative to the more widely used ^{238}U-^{206}Pb chronometer, which can be highly inaccurate for samples a few million years old, owing to uncertainties in the excess initial ^{234}U (hence, excess radiogenic ^{206}Pb) commonly observed in speleothems.

1 Introduction

Carbonates such as calcite and aragonite exist widely within the geological record, occurring as skeletal components of fossils such as corals, primary sedimentary deposits, secondary deposits such as speleothems, and as veins and fracture fillings. Such carbonates have the capacity to capture a range of information about past sea level and climate, regional tectonics etc., and are of particular significance because they are often amenable to direct radiometric dating based on the decay of U (Cheng et al., 1998; Edwards et al., 2003; Nuriel et al., 2012; Rasbury and Cole, 2009). Historically, this has been achieved mainly using ^{238}U-^{234}U-^{230}Th disequilibrium dating (e.g. Scholz and Hoffmann, 2008 and refs. therein), or less commonly ^{235}U-^{231}Pa disequilibrium dating (Cheng et al., 1998). These radiometric clocks are inherently limited to samples younger than the timescale over which the intermediate daughter used effectively returns to secular equilibrium; i.e. roughly 600,000 years for the ^{238}U-^{234}U-^{230}Th chronometer (Scholz and Hoffmann, 2008). Uranium-lead dating, being based on the accumulation of stable radiogenic Pb, does not suffer from this limitation, and has been applied for many decades to the dating of igneous and metamorphic accessory minerals (e.g. Heaman and Parrish, 1991). U-Pb dating has also been utilised in a more restricted way to date comparatively old sedimentary carbonates (e.g., Moorbath et al., 1987; Rasbury et al., 1997; Wang et al., 1998). More recently, U-Pb dating has been adapted and applied to geologically young carbonates as a means of circumventing the c. 600 ka limit of the ^{238}U-^{234}U-^{230}Th chronometer, opening up far more of the geological record (Bajo et al., 2012; Cliff et al., 2010; Getty et al., 2001; Li et al., 2014; Pickering et al., 2010; Richards et al., 1998; Roberts et al., 2017; Vaks et al., 2020; Woodhead et al., 2006; Woodhead and Pickering, 2012). However, the U-Pb system remains comparatively underutilised in this regard, and given the variety of sample material available and differences in laboratory set-up, it is unlikely that any implementation of the U-Pb system will be universally applicable. To this end, we document in detail a novel protocol for the U-Pb dating of carbonates by isotope dilution MC-ICP-MS recently used in a study of Siberian permafrost dynamics (Vaks et al., 2020).

2 Overview of the U-(Th)-Pb system and the motivation for a new method

The U-Th-Pb system is based on the twin decay chains of ^{238}U to ^{206}Pb and ^{235}U to ^{207}Pb, plus the decay chain of ^{232}Th to ^{208}Pb, together with unradiogenic ^{204}Pb. The ^{232}Th decay chain is not of direct relevance here as we are only considering systems that have sufficiently low ^{232}Th that ^{208}Pb can also be treated as unradiogenic; for our purposes, we consider ^{232}Th as negligible where $^{232}Th/^{238}U < 0.002$ (section 3.5). Owing to the insolubility of Th in many aqueous systems, many carbonates approximate a ^{232}Th-free system (e.g. Thomas et al., 2012; Vaks et al., 2013b).

Most previous U-Pb work on carbonates has focused on the ^{238}U-^{206}Pb system taking either a traditional solution-based isotope dilution approach where the samples are spiked with an isotopic tracer, dissolved, and then the U and Pb purified for analysis on a multi-collector MS, or have utilised *in situ* laser ablation analysis (e.g. Getty et al., 2001; Pickering et al., 2010; Roberts et al., 2017; Woodhead et al., 2006). We initially pursued the former route (Mason et al., 2013) as it offers better precision, e.g. < 0.1% uncertainty versus c. 0.6% or more by laser ablation on the $^{234}U/^{238}U$ ratio and < 1 % by isotope dilution versus 5-10% by laser ablation on the $^{238}U/^{206}Pb$ ratio, as well as the ability to date younger material with lower U and Pb concentrations (Cheng et al., 2013; Lin et al., 2017; Roberts et al., 2017; Spooner et al., 2016; Woodhead et al., 2006; Woodhead and Petrus, 2019). However, because relatively large samples (>100 mg) were required, miniaturisation of the columns to help control blanks was not an option, making the anion exchange chromatography both time consuming and challenging. Although reasonable Pb blanks (4 pg total Pb for a 2 ml resin bed) were attainable, this required secondary distillation of reagents, for example. We also experienced problems with the inconsistent purity of different anion exchange resin batches, with some batches yielding much higher Pb blanks (> 40 pg). Moreover, to avoid wasting effort and reagents on processing unradiogenic material, separate reconnaissance analysis would be required to first identify datable material, adding to the overall time needed to obtain an age. Having a simplified procedure that simultaneously maintained acceptable precision, side-stepped the Pb blank associated with anion exchange chromatography and minimised the time penalty for processing unradiogenic material to the point that separate reconnaissance U-Pb analyses were unnecessary, were significant motivations for developing a new method.

A caveat in U-Pb dating is that calculated U-Pb ages can strongly depend on the assumptions made regarding the initial state of the decay chains, especially initial $^{234}U/^{238}U$, $^{230}Th/^{238}U$, and $^{231}Pa/^{235}U$ ratios (Ludwig, 1977). For carbonates precipitated from fresh or sea waters, initial ^{230}Th and ^{231}Pa are likely to have been near absent owing to their insolubility in aqueous systems (Cheng et al., 1998; Edwards et al., 2003) and, thus, in practice do not present a major source of age uncertainty. However, initial ^{234}U can be strongly enriched with initial $^{234}U/^{238}U$ ratios as high as 7 to 12 times equilibrium known to occur (Kronfeld et al., 1994; Plagnes et al., 2002; Vaks et al., 2013b). If unaccounted for, the initial ^{234}U excess could lead to ^{238}U-^{206}Pb age inaccuracies of upwards of 2 Ma. For samples where the initial ^{234}U disequilibrium has not yet completely decayed (typically <2 Ma old), the initial $^{234}U/^{238}U$ ratio can be calculated from the measured $^{234}U/^{238}U$ ratio as part of the age calculation (here termed the ^{238}U-^{234}U-^{206}Pb chronometer), avoiding such inaccuracies. However, for older material, the initial $^{234}U/^{238}U$ ratio must be assumed in the age calculation (here termed the ^{238}U-^{206}Pb chronometer), potentially leading to significant inaccuracies in assessed ages. Where ages extend beyond the limit of the ^{238}U-^{234}U-^{206}Pb method, particularly where there is evidence for large variability in initial $^{234}U/^{238}U$ ratios, the ^{235}U-^{207}Pb chronometer could prove a powerful alternative dating tool. Such a situation was found in speleothems from Siberian caves (Vaks et al., 2020), which provided an additional motivation for developing the dating approach presented here. We pursue a solution-based method over laser ablation in order to obtaining precise $^{234}U/^{238}U$ measurements to effectively utilise the ^{238}U-^{234}U-^{206}Pb chronometer and because it represents a better prospect for detecting the tiny quantities of radiogenic ^{207}Pb necessary to apply the ^{235}U-^{207}Pb chronometer to samples a few Ma old.

A second caveat in U-Pb dating is that carbonates often contain an appreciable amount of initial (common) Pb that must be accounted for, usually requiring some form of isochron technique, though the choice of isochron used varies widely (e.g. Mason et al., 2013; Pickering et al., 2010; Woodhead et al., 2006). One approach (e.g. Roberts et al., 2017) is to use the intersection of an isochron in $^{238}U/^{206}Pb$ – $^{207}Pb/^{206}Pb$ (Tera-Wasserburg) space (or $^{238}U/^{206}Pb$ – $^{207}Pb/^{206}Pb$ – ^{204}Pb-^{206}Pb 'total' Pb space, Ludwig, 1998) with concordia to determine the $^{238}U/^{206}Pb_{rad}$ ratio ($^{20x}Pb_{rad}$ = radiogenic ^{20x}Pb) and, by extension, the age. However, this approach precludes an independent assessment of the $^{235}U/^{207}Pb_{rad}$ ratio, inhibiting the use of the ^{235}U-^{207}Pb chronometer. This strategy is further complicated by the calculation of concordia itself being sensitive to initial disequilibrium in the ^{238}U and ^{235}U decay chains. Alternatively, separate 2-D isochrons based on unradiogenic ^{204}Pb (e.g. Rasbury and Cole, 2009) can be used to independently correct common ^{206}Pb and common ^{207}Pb, permitting the usage of both the ^{238}U-^{206}Pb and ^{235}U-^{207}Pb systems. Nevertheless, using ^{204}Pb has the practical drawbacks of it being a low-abundance isotope and suffering an isobaric interference on ICP systems from instrumental Hg. However, in effectively ^{232}Th-free samples, the much more abundant ^{208}Pb can be used in place of ^{204}Pb as the unradiogenic Pb isotope (e.g. Mason et al., 2013). Implementing a streamlined ^{208}Pb-based approach, which obviously requires that ^{208}Pb be measured, was a further motivation for the development work presented here.

In summary, the objective of the present work is to present a new isotope dilution based method that streamlines sample preparation, particularly with regard to analysing blank-sensitive Pb/Pb and U/Pb ratios and which allows a ^{208}Pb-based approach to common Pb correction, such that the ^{238}U-^{234}U-^{206}Pb and ^{235}U-^{207}Pb chronometers can both be utilised, where the nature of the sample permits.

3 Protocol description

3.1 Protocol overview and reagents

The protocol comprises two distinct analytical procedures carried out sequentially, which in tandem are intended to provide the information necessary to calculate ^{238}U-^{234}U-^{206}Pb, ^{238}U-^{206}Pb, and ^{235}U-^{207}Pb ages, utilising ^{208}Pb for common Pb correction. The first procedure is concerned with determining the ^{238}U/^{206}Pb, ^{235}U/^{207}Pb, ^{208}Pb/^{206}Pb and ^{208}Pb/^{207}Pb ratios within a sample or part of a sample if more than one growth interval is present. The second procedure is concerned with analysing the same sample material to characterise residual ^{234}U/^{238}U disequilibrium, where the aforementioned U/Pb measurement indicates a ^{238}U-^{234}U-^{206}Pb age may be attainable.

The two procedures collectively require the following reagents, consumables etc. but will otherwise be described separately:

- 18.2 MΩ.cm water
- Quartz-distilled (or equivalent high-purity) 10 M HCl and dilutions of this
- Quartz-distilled (or equivalent high-purity) 16 M HNO_3 and dilutions of this
- Reagent grade 16 M HNO_3
- Bio-Rad AG-1 X8 anion exchange resin (or equivalent) 100-200 mesh
- 15 ml polypropylene bottles, acid cleaned for ~ 1 week in 1-2 M distilled HNO_3, then rinsed thoroughly with 18.2 MΩ.cm water
- 22 ml or 27 ml PFA vials, acid cleaned in hot, concentrated reagent grade HNO_3 for ~1 week, then refluxed in distilled 10 M HCl for at least 24 hours, and thoroughly rinsed with 18.2 MΩ.cm water after each acid stage
- 2 ml Bio-Rad polyprep columns (or equivalent), acid cleaned for ~1 week in 1-2 M distilled HNO_3, then rinsed thoroughly with 18.2 MΩ.cm water

- CRM145 (New Brunswick Laboratory) natural U, or equivalent U isotopic reference material.
- Single element Tl standard

The quartz-distilled acids used are comparable to commercially available ultra-pure acids – i.e. ppt or lower concentrations for the analytes of interest. The 18.2 MΩ.cm water used is approaching absolute purity for the analytes of interest (e.g. < 20 ppq for Pb). All dilutions of distilled acids were prepared with 18.2 MΩ.cm water.

3.2 U-Pb measurements

Collected samples were first sawn using a diamond-coated wire saw to reveal their internal structure and provide access to the stratigraphic horizons or growth domains of interest. Clean carbonate subsamples weighing between c. 50-500 mg were then cut from specific stratigraphic horizon or growth domains using a small diamond circular saw and transferred to acid-cleaned 15 ml polypropylene bottles. These subsamples were then sonicated repeatedly in 18.2 MΩ.cm water until no suspended particles were visible, rinsing between each wash. The subsamples were then twice acid cleaned for a few minutes in distilled 2 % HNO_3 with sonication to remove any residual dirt and surface contamination. Following each wash, the subsamples were thoroughly rinsed with 18.2 MΩ.cm water and sonicated to ensure removal of any residual acid and dislodged surface material. Each acid wash was removed before the acid was consumed, to prevent adsorption of dissolved ions back on to the surface of the sample. Where sample material was abundant, we used initial subsample masses of a few hundred milligrams for ease of handling during cleaning, but this mass was reduced where material was limited. The subsample mass after cleaning should be no smaller than c. 10 mg. Cleaned subsamples were then stored until the day of analysis.

Subsamples were usually taken from specific sample domains without prior characterisation of the U/Pb system. Instead, surplus subsamples were prepared from a number of different samples or sample domain to provide the flexibility to re-target the subsequent analytical session, as it became apparent which material was radiogenic and which was not.

On the day of analysis, one to two drops of a mixed ^{204}Pb-^{230}Th-^{236}U (~30 µL drop volume, c. 15 pg µL^{-1} ^{236}U, c. 1 pg µL^{-1} ^{204}Pb, and 0.5 pg µL^{-1} ^{230}Th; full isotopic calibration is given in Mason et al., 2013) spike in c. 2 M HNO_3 was added directly to the acid cleaned carbonate subsample and gently agitated to mix as the spike dissolved the subsample. Cleaned subsamples were not weighed in order to minimise handling. Instead, the mass of $CaCO_3$ from the subsample used was in excess of the HNO_3 in the spike, such that the spike can dissolve sample material until the contained HNO_3 is consumed, thereby fixing the mass of sample material dissolved (typically 3-8 mg) to c. 10 % of the added spike mass. Although not critical to the age calculation, this allowed the absolute sample U concentration to be estimated without weighing, based on the amount of sample expected to dissolve in a given mass of spike. Once visible reaction with the spike was complete, the solution was diluted to around 15 ml with 18.2 MΩ.cm water, thoroughly shaken to homogenise and then immediately analysed, with no preconcentration of U and Pb. Dilution to c. 15 ml provides sufficient solution to check instrument set-up (see below) prior to analysis, allows replicate analyses if needed, and mitigates matrix loading on the instrument.

Analyses were performed on a first generation Nu Plasma MC-ICP-MS (Belshaw et al., 1998) using the collector configuration given in Table 1 and described further below. The instrument was fitted with a set of 'B-type' Ni cones reserved for very low level Pb work. Sample introduction was via a DSN100 (Nu Instruments) desolvator using either a c. 50 µL min^{-1} or 75 µL min^{-1} self-aspirating PFA nebuliser (ESI). The instrument and desolvator were slightly modified by replacing the gas and sample lines with acid cleaned PFA to lower the long-term instrumental Hg background, reducing the ^{204}Hg interference on ^{204}Pb. The 'Hot Gas' feed to the DSN100 spray chamber was also disconnected and sealed.

At the beginning of an analytical session the instrument was prepared by cleaning the desolvator and sample lines with 10 % HNO_3, 2 % HNO_3, and 18.2 MΩ.cm water. The Ni cones were also gently cleaned by rinsing with DI water prior to use to remove excessive Ca build-up from the skimmer orifice from previous use, however, as far as possible, the surface coating on the cones was not disturbed. The instrument was then initially tuned and optimised with c.100 ppt Tl solution and 5 ppb CRM145 U solution (both in 2% HNO_3). Pb was avoided to prevent re-contamination of the instrument and, sufficient Pb-blank was present in the Tl solution to identify the Pb peaks. Instrumental Pb background could then be further reduced by temporarily lowering the auxiliary gas flow (to c. 0.5 L min^{-1}) with RF power at 1300 Watts, allowing the plasma to run hot to 'evaporate' residual Pb from the instrument interface and then using relatively cool running conditions (auxiliary gas flow of 1.15 L min^{-1} and 1200-1250 Watts RF power). In some instances, this reduced the Pb background by a factor of >10×, without major loss of sensitivity. The instrument was then left for several hours until Hg adsorbed on the interface etc. had evaporated and the Hg background had stabilised.

After the initial tuning and optimisation of the instrument on the dilute Tl and U solutions, instrument settings were checked on actual samples. At the beginning of an analytical session, particularly after the cones had been cleaned, it was often necessary to refocus the zoom optics to obtain optimal flat-topped peaks on the matrix-heavy samples. The DSN100 membrane gas flow was also retuned to suppress a molecular interference observed to overlap the Pb peaks, particularly ^{208}Pb, but with its peak centres offset by c. 0.15 AMU to the low-mass side of the Pb peaks. The c. 0.15 AMU mass offset generally made the superimposed interference peaks obvious, such that the DSN100 'membrane' gas flow could be adjusted while performing a mass scan until the superimposed peak had been largely eliminated. Based on the mass offset, the interference is a molecular of a mid-mass element; $Sr_2O_2^+$ is suspected based on the group 2 element-rich matrix and the relative magnitude at masses 208, 207, 206 etc. The signal intensity of this interference varies over several orders of magnitude with the DSN100 'membrane' and 'hot' gas settings, but has been observed to be largely eliminated by disabling the 'hot' gas flow and setting the 'membrane' gas flow slightly below the optimum value for Tl signal intensity on the pure

Tl solution. Where a small residual interference was seen (only apparent on ^{208}Pb and occasionally up to 10 % of the ^{208}Pb signal, but only on highly radiogenic samples with little ^{208}Pb), the mass offset between the Pb and interference beams meant the extreme high-mass side of the Pb peaks was effectively resolved from the interference, proving peak shape was optimal. No correction was made for the $Sr_2O_2^+$ interference and the method is based on its effective elimination. ^{208}Pb, although not directly used for age calculation, forms the basis of the common Pb correction (section 3.5), so at this stage, an assessment of any residual interference was made in terms of its impact on the common Pb correction. Where no residual interference on ^{208}Pb was observed, or where it was considered irrelevant (e.g. for material with almost no common Pb), the instrument was set to analyse on the centre of the Pb peaks for optimum stability. Where this was not the case, particularly where ^{235}U-^{207}Pb ages were targeted (owing to the larger common Pb correction on ^{207}Pb), the instrument was set to analyses on the extreme high mass side of the Pb peak flats where the interference is effectively resolved. No evidence of interferences on U has been observed.

Table 1. Collector configuration for U-Pb analysis.

	Axial							low mass	Integration time
step	**DVM6**	**DVM7**	**DVM8**	**IC0**	**DVM9**	**IC1**	**DVM10**	**IC2**	
0				208		206		204	10s
1				207					10s
2				206		204		202	10s
3				204		202			10s
4		238		236	235				10s
5	238		236	235					10s
6				232		230			10s

DVM' collectors are Faraday collectors, 'IC' collectors are electron multiplier ion counters. Step 6 is optional and can be omitted if the ^{232}Th is already known to be negligible in the sample (e.g. from a prior attempt at U-Th dating).

Analyses were carried out in a six-step routine with the magnet switched successively between steps (Table 1) for 10 or 15 repetitions. In steps 0-3 ^{208}Pb, ^{207}Pb, ^{206}Pb, ^{204}Pb+^{204}Hg, and ^{202}Hg were measured on three ion-counters (ICx collectors in Table 1) separated by Faraday collectors (DVMx collectors in Table 1), which are not used in these steps owing to the small size of the Pb signals. The relative gains of the three ion counters were determined based on the successive measurement of the mass-204$^+$ beam on each ion counter during the analysis. ^{207}Pb is measured entirely dynamically owing to the ion counter spacing. Ion counter gains and dynamic ratios involving ^{207}Pb etc. were calculated with no beam interpolation between steps assuming a steady-state measurement. ^{202}Hg was measured and used to correct for the ^{204}Hg interference (typically c. 15% of the total 204$^+$ beam with the quantity of spike used here). In steps 4-5 ^{238}U was measured on a Faraday collector, with ^{235}U and ^{236}U measured alternately on both Faraday and ion counter; the intention being that this gives the option of using the Faraday/Faraday ^{238}U/^{235}U ratio or the Faraday/ion counter ^{238}U/^{235}U ratio (using the ^{236}U to calibrate the ion counter gain as needed) depending on ^{235}U signal intensity. An optional step with ^{232}Th in IC0 and ^{230}Th in IC1 (Table 1) can be added where estimation of sample ^{232}Th/U ratio is required (as a check ^{232}Th is negligible), if this is not already known (e.g. from a prior attempt at U-Th dating). Mass fractionation for U was determined from the measured ^{238}U/^{235}U ratio of the samples and an assumed natural value of 137.75 (based on data for carbonates precipitated from surface waters summarised in Hiess et al., 2012 from Stirling et al., 2007 and Weyer et al., 2008). Mass fractionation for Pb was also estimated based on the measured ^{238}U/^{235}U ratio but with a + 2 ‰/AMU offset applied based on previous characterisation of the U-Pb mass fractionation behaviour of this instrument (Mason and Henderson, 2010). In these tests, the offset between U and Pb fractionation was observed to be nearly constant over a wide range of fractionation values, including those seen for the matrix-rich samples analysed here. Samples were washed out with 10 % and 2 % distilled HNO_3 while the next sample was spiked. Analysis time was around 15 minutes.

Instrument settings were checked periodically during the analytical session to ensure peak centring, peak shape, and suppression of interferences was maintained. Special care was taken when highly radiogenic material capable of yielding precise ages was encountered and, when the instrument was set to measure on the extreme high mass side of the Pb peak flats. The DSN100 was re-cleaned with 18.2 MΩ.cm water as required to remove U and Pb background or when sensitivity dropped due to Ca-loading of the membrane.

Explicit procedural blank corrections were not made to the U-Pb analyses owing to the measured blank signals being below the instrumental detection limit. However, based on a typically observed detection limit for total Pb of c. 20 ppq (based on ^{208}Pb), an upper limit for the total procedural Pb blank can be estimated at c. 0.3 pg.

3.3 Choice of tracer solution

We use a mixed ^{236}U-^{230}Th-^{204}Pb tracer for isotope dilution (calibration in Mason et al., 2013). Using the non-radiogenic ^{204}Pb as tracer allows the measurement of the radiogenic ^{206}Pb and ^{207}Pb and it is the least abundant of the four stable Pb isotopes in the samples. ^{204}Pb is also more easily obtainable than artificial ^{205}Pb and ^{202}Pb. The instrumental Hg background also makes the small unspiked ^{204}Pb signal unsuitable as a monitor for common Pb without preconcentration, so spiking with ^{204}Pb does not sacrifice any sample information that would otherwise have been obtainable. Moreover, for ^{238}U-^{234}U-^{206}Pb chronology, using a tracer with ^{204}Pb paired with artificial ^{236}U means that the critical ^{238}U/^{206}Pb ratio is determined from the ^{238}U/^{236}U and ^{206}Pb/^{204}Pb ratios, so it is relatively insensitive to instrumental mass fractionation due to the mass difference for the natural/spike isotope being the same for both U and Pb. For ^{238}U-^{234}U-^{206}Pb chronology on the instrument used, ^{204}Pb is also more favourable than ^{205}Pb because it can be collected simultaneously on the ion-counters with ^{206}Pb, whereas ^{205}Pb cannot (Table 1); ^{205}Pb may, however, represent a better option for other hardware configurations. The disadvantage of using ^{204}Pb is that sample (and blank) ^{204}Pb must be corrected for, but this correction can be reduced by adding sufficient spike ^{204}Pb that the sample contribution is minor. In our case, the sample to spike weight ratio is limited to about 0.1 by the availability of the HNO_3 in the spike to dissolve sample. For most analyses, this corresponds to >98.5 % ^{204}Pb arising from the spike, with many of the highly radiogenic analyses (i.e. the fractions for which precise ages can be obtained) having >99.8% of the ^{204}Pb originating from the spike. Any age bias introduced in accounting for the sample ^{204}Pb is therefore likely to be at the ‰ level and less than the typical analytical precision on the ^{238}U/^{206}Pb and ^{235}U/^{207}Pb ratios.

^{230}Th is included in the tracer to provide the option to measure ^{232}Th as a check that ^{208}Pb is unradiogenic. ^{230}Th is preferable to artificial ^{229}Th on the instrument used because of the 2 AMU spacing of the ion counters (Table 1). Again sample ^{230}Th needs to be accounted for, but for samples in the U-Pb age range, sample ^{230}Th is likely to be close to equilibrium with ^{234}U. Moreover, the ^{232}Th only needs to be measured semi-quantitatively as a check of the applicability of the method, and is not used in the age calculation.

3.4 ^{234}U/^{238}U measurements for ^{238}U-^{234}U-^{206}Pb chronology

Where the U-Pb data indicated a particular sample domain is radiogenic and potentially young enough to retain measurable residual ^{234}U disequilibrium, the domain was additionally analysed for the ^{234}U/^{238}U ratio for ^{238}U-^{234}U-^{206}Pb chronology. Sample aliquots of up to about 0.2 g were dissolved and purified to obtain U cuts. As far as possible these aliquots comprised the residual solution and remaining carbonate from the U-Pb analysis, so that the U/Pb and ^{234}U/^{238}U measurements were made on as close to the same material as possible. Dissolution was by addition of 0.2 ml of 10 M HCl to the residual solution + residual carbonate. After obvious reaction had ceased, the solution was transferred to clean 22 ml or 27 ml PFA vials and evaporated to dryness. The sample was then converted to chloride form by adding 1 ml 10 M HCl and again evaporating to dryness. Samples were then dissolved in 1 ml of 10 M HCl for loading onto columns for separation of U. Purification used 2 ml Bio-Rad polyprep columns and an AG1X8 anion exchange resin bed of 2 ml. Resin was batched pre-cleaned by suspending it in either 18.2 MΩ.cm H_2O or dilute HCl, allowing it to settle and decanting any residual suspended fines 8-10 times. Resin was then loaded into the column and cleaned sequentially with ~10 ml (column reservoir filled) 18.2 MΩ.cm H_2O, 10 M HCl and 18.2 MΩ.cm H_2O. The resin was then conditioned with two 4 ml aliquots of 10 M HCl, and the sample loaded and matrix Ca eluted with 2 x 5 ml aliquots of 10 M HCl. Sample U was eluted with 2 x 5 ml aliquots of 18.2 MΩ.cm water and collected in the origin PFA vial (which was rinsed first with 18.2 MΩ.cm H_2O to remove the bulk of any sample Ca residue). The purified U was measured on the same instrument, with the ^{234}U and ^{238}U respectively measured on ion counter and Faraday collectors. Standard bracketing with CRM145 (CRM112a) was used to correct both for mass fractionation and ion counter gain.

Owing to the very small ^{234}U blank signal, the ^{234}U/^{238}U ratio of the U blank could not be meaningfully measured, so no blank correction was routinely applied to the ^{234}U/^{238}U measurements. The typical procedural blank for the ^{234}U/^{238}U ratio measurement was c. 50 pg U.

Purification of the U fraction is required because the $^{234}U/^{238}U$ ratio must be measured to a higher precision than the $^{238}U/^{206}Pb$ ratio. This requires preconcentration of the U to obtain a sufficiently large ^{234}U signal to ideally obtain better than 1 ‰ precision. Uranium, however, is generally less blank sensitive than Pb so the ion exchange procedure is relatively straightforward. Moreover, only those samples for which a $^{234}U/^{238}U$ measurement will be beneficial need be processed.

3.5 Non-radiogenic Pb correction and Age calculation

To obtain an accurate age, it is necessary to account for any non-radiogenic Pb (blank and sample common Pb) in an analysis. The preferred method used here is to employ a 2-D isochron-type approach in which the ^{238}U-(^{234}U)-^{206}Pb and ^{235}U-^{207}Pb systems are independently corrected for common Pb, respectively in $^{208}Pb/^{206}Pb$-$^{238}U/^{206}Pb$ and $^{208}Pb/^{207}Pb$-$^{235}U/^{207}Pb$ isotope space; example plots are shown in sections 5 and 6. For a ^{232}Th-free system, subsamples of the same age should define a mixing trend between the common $^{208}Pb/^{20x}Pb$ composition falling on the $^{208}Pb/^{20x}Pb$ axis (i.e. where $^{23y}U/^{20x}Pb = 0$) and the radiogenic $^{23y}U/^{20x}Pb$ composition falling on the $^{23y}U/^{20x}Pb$ axis (i.e. where $^{208}Pb/^{20x}Pb = 0$, assuming all ^{208}Pb is common), where ^{20x}Pb is the daughter of ^{23y}U. The common Pb correction can then either be made by fitting a regression line through the data to estimate the $^{23y}U/^{20x}Pb_{rad}$ ratio (the intersection with the $^{23y}U/^{20x}Pb$ axis), or a regression line can be fitted to estimate the common $^{208}Pb/^{20x}Pb$ composition (the intersection with the $^{208}Pb/^{20x}Pb$ axis), which can then be used to correct each U-Pb analysis based on its measured $^{208}Pb/^{20x}Pb$ ratio. The latter option is preferred here because it allows age-independent scatter in the radiogenic $^{23y}U/^{20x}Pb$ ratio arising from differences in initial disequilibrium state to be accommodated; the estimation of the common Pb composition is insensitive to such scatter in the radiogenic composition providing that any regression is anchored by relatively unradiogenic analyses. Correcting measurements individually also allows for the pairing of each corrected U-Pb analysis with a corresponding $^{234}U/^{238}U$ measurement, capturing any additional information encoded in the $^{234}U/^{238}U$ ratio. For regressions we use the method of York (1969).

In practice, when dealing with a set of related material (e.g. different growth domains in the same speleothem, or different speleothems from the same cave), isochrons for every sample domain to be dated were not constructed at the outset to attempt to minimise analytical effort. Instead, data were acquired until subsets of material approximating a mixing trend between the radiogenic and common Pb end members could be identified (e.g. an unradiogenic layer stratigraphically bracketed by more radiogenic layers) and regressed to estimate the common Pb composition. This estimate was then used as the basis for the common Pb correction in the wider data set for the related material under consideration. Where samples proved complex in terms of their U-Pb systematics, additional analyses were added to provide further characterisation and to allow true isochrons to be constructed if needed.

In reality, ^{232}Th will be present in trace amounts, with the resulting trace ^{208}Pb$_{rad}$ shifting the ^{208}Pb/^{20x}Pb ratio to slightly higher values than if ^{232}Th was absent, slightly biasing the calculated ^{23y}U/^{20x}Pb$_{rad}$ ratio. We consider the bias to be acceptable without correction for ^{232}Th where ^{232}Th/^{235}U < 0.276 (equivalent to ^{232}Th/^{238}U < 0.002). This threshold corresponds to a maximum bias in the ^{235}U/^{207}Pb$_{rad}$ ratio of c. 0.6 %, or c. 1/3 of the typical analytical precision on the measured ^{235}U/^{207}Pb ratio; the ^{238}U/^{206}Pb$_{rad}$ ratio is much less sensitive owing to the smaller common Pb correction on ^{206}Pb. Setting this limit on ^{232}Th in terms of the Th/U ratio has two effects in terms of ^{208}Pb/^{20x}Pb-^{23y}U/^{20x}Pb space. Firstly, it constrains the ^{208}Pb$_{rad}$/^{20x}Pb$_{rad}$ ratio to be close to zero by limiting the ratio of the respective parent isotopes, such that an accurate radiogenic ^{23y}U/^{20x}Pb composition can still be obtained by extrapolation to the ^{23y}U/^{20x}Pb axis (i.e. to ^{208}Pb/^{20x}Pb = 0). Secondly, it constrains compositions with a low U/Pb ratio to also have a low Th/Pb ratio, such that extrapolation to the ^{208}Pb/^{20x}Pb axis (^{23y}U/^{20x}Pb = 0) to obtain the common Pb composition will also correspond to a ^{232}Th-free composition free of radiogenic ^{208}Pb.

For relatively young samples in which ^{234}U/^{238}U disequilibrium can still be quantified, model ^{238}U-^{234}U-^{206}Pb ages were calculated from each corresponding pair of U-Pb and ^{234}U/^{238}U analyses, using the estimated common ^{208}Pb/^{206}Pb ratio to correct for the total non-radiogenic ^{206}Pb, based on the measured ^{208}Pb/^{206}Pb ratio. In this instance, the initial ^{234}U/^{238}U ratio was calculated from the measured ^{234}U/^{238}U ratio as part of the age calculation analogous to U-Th dating. For older material, model ^{238}U-^{206}Pb ages were calculated using an assumed initial ^{234}U/^{238}U ratio (which was chosen arbitrarily in the present work for illustrative purposes only). Model ^{235}U-^{207}Pb ages were calculated in an equivalent way correcting for the total non-radiogenic ^{207}Pb in the analysis based on the measured ^{208}Pb/^{207}Pb ratio and the estimated common ^{208}Pb/^{207}Pb ratio. Where ^{235}U-^{207}Pb ages were calculated but no corresponding ^{238}U-^{234}U-^{206}Pb age could be determined, the ^{238}U→^{206}Pb system was solved for the initial ^{234}U/^{238}U ratio using the calculated ^{207}Pb/^{235}U age.

Alternatively, Tera-Wasserburg space was used in which the age is determined without explicit common Pb correction, based on the intersection of an isochron with concordia (e.g. Roberts et al., 2017). This approach, however, is not favoured by us as it does not allow separate evaluation of the ^{238}U-(^{234}U)-^{206}Pb and ^{235}U-^{207}Pb systems (and often involves assumptions about initial disequilibrium in order to calculate concordia) but is utilised here where necessitated to compare independently obtained data (e.g. when ^{208}Pb was not measured).

Model ages and concordia were calculated using an in-house implementation of the general decay equations given by Faure (1986), in which the decay chains are simplified to ^{238}U → ^{234}U → ^{230}Th → ^{226}Ra → ^{206}Pb and ^{235}U→ ^{231}Pa → ^{207}Pb. Initial ^{230}Th and ^{231}Pa were assumed to have been absent and initial ^{226}Ra was assumed to have been at equilibrium. Decay constants used were: ^{238}U: 1.55125×10^{-10}, ^{234}U: 2.82203×10^{-6}, ^{230}Th: 9.17055×10^{-6}, ^{226}Ra: 4.33488×10^{-4}, ^{235}U: 9.8485×10^{-10}, ^{231}Pa: 2.11583×10^{-5}, ^{232}Th: 4.9475×10^{-11} (Cheng et al., 1998, 2013; Steiger and Jäger, 1977) Age uncertainties were determined using a Monte Carlo approach to propagate analytical uncertainty and uncertainties arising from initial ratios such as the common Pb composition and initial U isotopic composition. A natural ^{208}Pb/^{204}Pb ratio of 37.1±10 (95% confidence level) was assumed when accounting for sample ^{204}Pb in the isotope dilution calculation; the large uncertainty is to cover reasonably foreseeable terrestrial isotopic variations. As part of the isotope dilution calculation the spike ^{204}Pb proportion is output so that analyses with an excessive sample ^{204}Pb contribution can be identified. For most analyses, >99% of the total ^{204}Pb originated from the tracer. Blank Pb is not separately corrected for and is dealt with as part of the total non-radiogenic Pb correction, however, given a number of analyses have yielded >99% radiogenic ^{206}Pb, the Pb blank can be considered a generally minor source of non-radiogenic Pb.

4 Protocol validation methodology and sampling

In the absence of suitable well-characterised carbonate reference materials during the period of method development, the validation of the new procedure required means other than the direct analysis of reference materials. As an alternative, we set four independent validation tests for the new method:

1) The new method must be able to produce data/ages consistent with measurements by a conventional isotope dilution approach with purification of U and Pb – i.e. not removing the matrix must have no appreciable impact on the resulting data/ages.
2) The method must be able to generate U-Pb ages that vary systematically with stratigraphic order in samples where the successive growth intervals are resolvable.
3) In samples where the common Pb correction permits, the method must be able to generate concordant ^{238}U-^{234}U-^{206}Pb and ^{235}U-^{207}Pb ages.
4) The method should replicate data obtained independently in a different laboratory.

These four tests have been performed on three samples: ASH-15, SLL10-6, and JOHO-1. A fourth sample, SB_pk142 is analysed as a case study for the application of the ^{235}U-^{207}Pb chronometer.

ASH-15 is a calcite flowstone comprising a younger relatively thin brownish layer overlying an older, more massive yellowish layer (Fig. 1), and originates from Ashalim cave, Negev Desert, Israel. The massive yellow layer has previously been independently analysed at the University of Melbourne (Vaks et al., 2013a) and the University of Oxford (Mason et al., 2013) and has an age of c. 3 Ma and a U concentration of c. 1.5 ppm; ^{232}Th is negligible (Mason et al., 2013). The latter data set, obtained with purification of the U and Pb from the matrix, is compared to new data obtained using the new protocol (i.e. without matrix removal) as a preliminary test of not removing the matrix.

SLL10-6 is a high-U (6 to 43 ppm) calcite stalagmite from Ledyanaya Lenskaya cave, Siberia (Vaks et al., 2020). The sample comprises several distinct layers designated from A to G, in order of increasing stratigraphic age and mostly separated by visible hiatuses (Fig. 1). All seven stratigraphic layers have been analysed using the new protocol. Five subsamples each from the F and G layers have also been purified and analysed using the method of Mason et al. (2013). This provides control data, such that the reproducibility of the F and G ages, with and without matrix separation, can be tested. The multilayer nature of the sample is additionally used to test the ability of the new method to produce ages in stratigraphic order, while the high-U nature of the sample makes it suitable for testing concordance of ^{238}U-^{234}U-^{206}Pb ages and ^{235}U-^{207}Pb ages. Previous ^{232}Th/^{238}U measurements from this sample and other samples from the same cave (Vaks et al., 2013b) give a maximum ^{232}Th/^{238}U ratio of 1.6×10^{-3} and indicates the radiogenic ^{208}Pb contribution is insignificant.

JOHO-1 (Fig. 1) is a fault vein calcite from the Middle East with a relatively low bulk U concentration of 0.3-0.5 ppm. The fault vein has been analysed independently at the University of Oxford using the new protocol described and at the NERC Isotope Geoscience Laboratory (NIGL), Keyworth, UK, by laser ablation ICP-MS, following the methods of Roberts et al. (2017). The laser ablation analyses targeted a domain that included material with a much higher U concentration (up to 25 ppm). The sample is used to test the new protocol via inter-laboratory comparison.

Figure 1: Samples: ASH-15 is a calcite flowstone from Ashalim Cave, Negev Desert. It comprises a lower yellow-orange unit c. 3 Ma old and a younger brown unit not analysed here. SLL10-6 is a calcite stalagmite from Ledyanaya Lenskaya Cave, Siberia. It comprises several layers designated A to G in order of increasing stratigraphic age, each apparently separated by a hiatus. SB_pk142 is an aragonitic speleothem comprising a flowstone that has merged with and encased two stalactites. The prominent iron oxide-stained layer (dashed line) separating stratigraphically older and younger parts of the sample should be noted. The flowstone portion of the sample shows prominent lamination (sub-horizontal as viewed). The larger of the two stalactites forms the relatively featureless portion of the sample (with saw cuts on the left image), but some growth laminae (near vertical as viewed) can be seen on the right image, and these pass continuously, but with sharp inflection, in to the flowstone portion of the sample below the iron oxide-stained layer, indicating the stalactite and lower part of the flowstone are stratigrahically equivalent. Remnants of a smaller stalactite form the extreme top left corner of the sample on the left image. The portion of the flowstone above the iron oxide-stained layer appears to encase the stalactites and, hence, is mostly younger than them. Arrows indicate growth direction. JOHO-1 is a calcite fault vein from the Middle East.

SB_pk142 (Fig. 1) is an aragonite speleothem from Botovskaya cave, Siberia. The sample consists of part of a stalactite that has merged in to flowstone, with the remains of a second smaller stalactite (now encased by the flowstone portion of the sample) on one corner of the sample, and traces of reddish-brown clay on the stratigraphic base of the flowstone. The sample contains two stratigraphic domains separated by a prominent iron oxide-stained lamina, possibly representing a hiatus. Multiple subsamples from both stratigraphic domains have been analysed using the new method. A notable feature of speleothems from this cave is the large and variable ^{234}U excess, with known initial ^{234}U/^{238}U ratios ranging between 3.4 and 8.1 times equilibrium (Vaks et al., 2013b, 2020). This sample is used as an example application of the ^{235}U-^{207}Pb chronometer to a cave system where the ^{238}U-^{206}Pb chronometer is problematic. Aragonite samples from Botovskaya cave show consistently low ^{232}Th/^{238}U ratios ($<2\times10^{-4}$, Vaks et al., 2013b)), such that the radiogenic ^{208}Pb contribution is insignificant.

Detailed representative sample petrography for samples from Ledyanaya Lenskaya and Botovskaya caves, as well as details of the caves themselves are given in Vaks et al. (2013b, 2020).

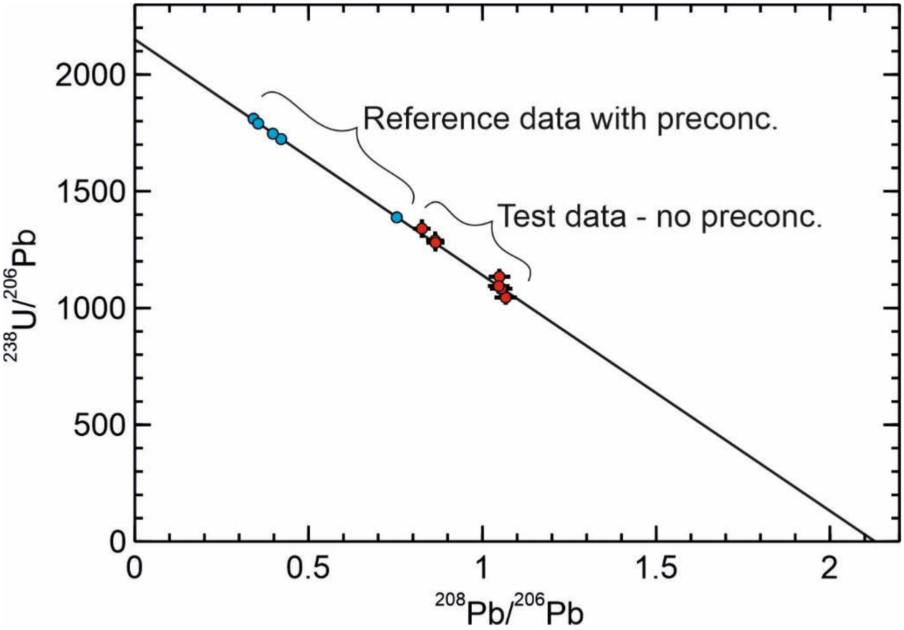

Figure 2: Preliminary data from ASH-15 showing comparison of data obtained with the new method with no preconcentration with published data obtained with preconcentration (Mason et al., 2013). The critical result is that the data produced using the new method are co-linear with the data obtained with preconcetration and define a common isochron. The intersection of the isochron with the ^{208}Pb/^{206}Pb axis gives the common ^{208}Pb/^{206}Pb ratio and the intersection with the ^{238}U/^{206}Pb axis gives the ^{238}U/^{206}Pb$_{rad}$ ratio providing the ^{208}Pb is entirely unradiogenic.

5 Protocol validation results

5.1 ASH-15

Results for ASH-15 are given in Table 2 and Fig. 2. These analyses were intended as a preliminary test that the new U-Pb measurement procedure without matrix separation produces data consistent with published data (Mason et al., 2013) obtained using the same spike but with purification of U and Pb from the matrix. The new analyses are slightly less radiogenic than the analyses of Mason et al. (2013), however, they are not exact replicates of the same subsamples, so some variation in the proportion of common Pb can be expected. The critical feature is that the data with and without matrix separation are co-linear defining a common isochron (Fig. 2) and are therefore consistent.

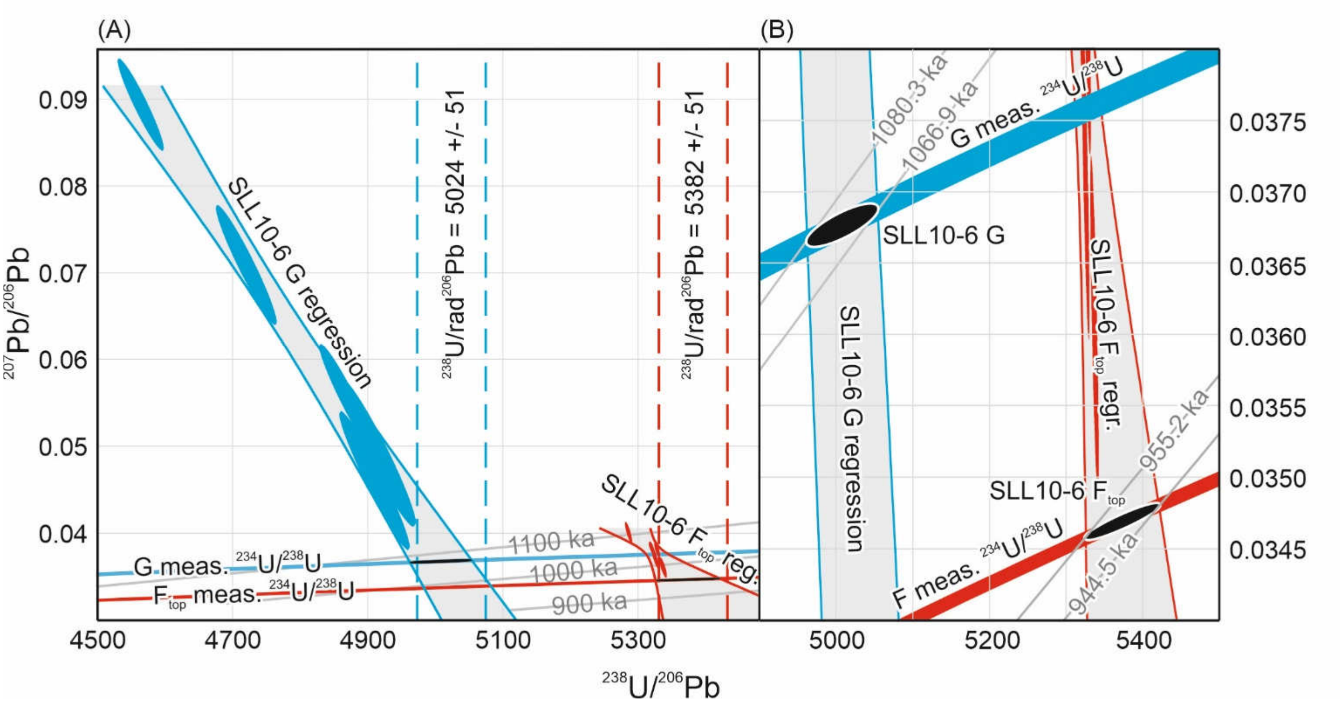

Figure 3: A) Modified Tera-Wasserburg diagram showing the control data for SLL10-6 G and F layers obtained with purification of the U and Pb from the matrix following the method of Mason et al. (2013). Because the initial ^{234}U/^{238}U ratio is not known *a priori* a unique concordia curve appropriate to each sample layer cannot be defined. Instead, two sets of tie-lines (the sub-horizontal curves) connecting concordia curves (not shown) with different initial ^{234}U/^{238}U ratios are plotted. The first set connects points of equal ^{234}U/^{238}U ratio for values corresponding to the mean measured ^{234}U/^{238}U ratio (± uncertainty) for the F and G layers. The second set of tie lines are age contours connecting points of equal age. The interpreted radiogenic ^{238}U/^{206}Pb and radiogenic ^{207}Pb/^{206}Pb ratios must simultaneously satisfy the tie-line corresponding to the measured ^{234}U/^{238}U ratio, and the mixing trend with common Pb defined by the regression fits (grey shaded bands) to the measured U-Pb data – i.e. the intersections shown with the black ellipses. The age is then defined by where the intersection falls in relation to the age contours. The vertical dashed lines indicate the radiogenic ^{238}U/^{206}Pb ratios interpreted from regression intercepts in ^{208}Pb/^{206}Pb-^{238}U/^{206}Pb isotope space (not shown but equivalent to Fig. 6a) as a cross-check, and are consistent with the aforementioned intersections. B) Enlargement of the intersections between the regression fits to the measured data and the equal ^{234}U/^{238}U tie-lines for the sample measured ^{234}U/^{238}U ratios. Age contours correspond to the maximum and minimum ^{238}U-^{234}U-^{206}Pb age defined by the intersections for each sample layer. Calculations assume ^{238}U/^{235}U=137.75, no initial ^{231}Pa or ^{230}Th and equilibrium initial ^{226}Ra.

5.2 SLL10-6

Control data for the F and G layers obtained with purification of U and Pb from the matrix following the method of Mason et al. (2013) are given in Table 2 and Fig. 3. Data and ages obtained using the new analytical methodology for all layers of SLL10-6 are also given in Table 2, and Fig. 4. Blanks for the control data were 4.1 pg Pb, 24.8 pg U for the F layer and 42.0 pg Pb, 18.8 pg U for the G layer. Control data are blank corrected.

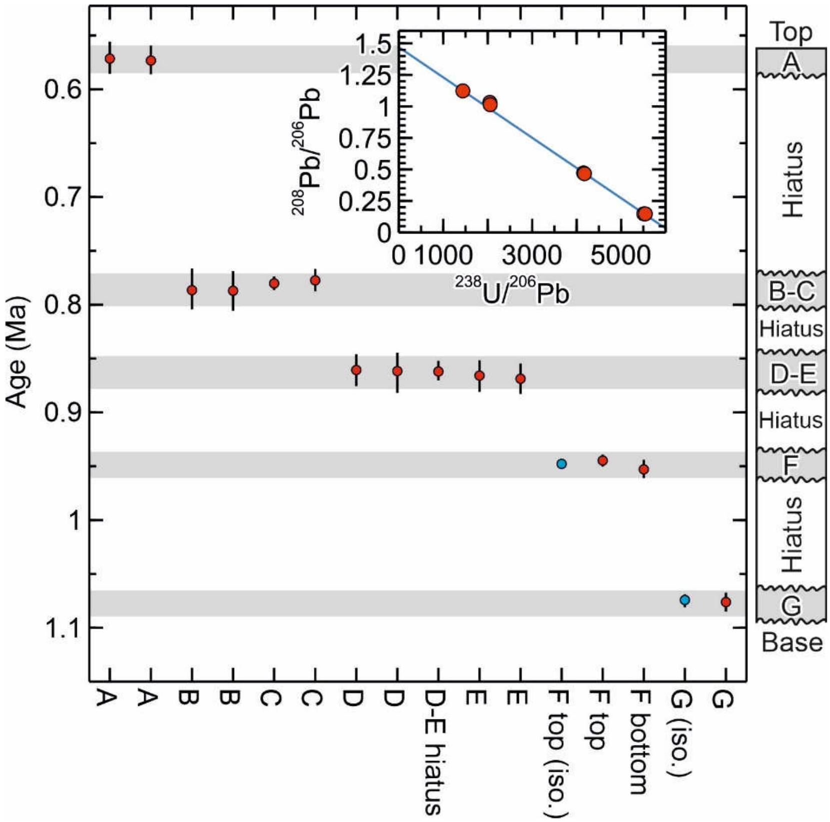

Figure 4: Summary data for SLL10-6 showing the replication of the ages from the layers F & G obtained using the method of Mason *et al.* (2013) (ages with 'iso.' label) with the ages obtained using the new method, and the consistency of the ages produced with the new method with the stratigraphic order of the sampled layers. The inset shows isotopic data from the layers B & C which includes some of the least radiogenic analyses obtained from this cave, and were used to help constrain the common ^{208}Pb/^{206}Pb to c. 1.5 (^{208}Pb/^{206}Pb axis intercept). The rather low (radiogenic) common ^{208}Pb/^{206}Pb ratio is considered to have resulted from ingrowth of ^{206}Pb in the source of the common Pb (presumably the cave host rock), prior to the growth of SLL10-6.

In terms of the measured ^{238}U/^{206}Pb ratio, for the F layer, the control data are markedly more precise than the data obtained using the new protocol (typical relative uncertainty of ± 0.075 % versus ± 0.9%; Table 2), but the precision is more similar for the G layer (0.8 % versus 1.2 %) owing to the larger Pb blank correction in the G layer control data. The control data yield ^{238}U-^{234}U-^{206}Pb isochron ages of 1073.6 ± 6.7 ka and 949.9 ± 5.4 ka (95% conf.) respectively for the G layer and the upper part of the F layer. The corresponding ages for the G layer and the upper part of the F layer obtained using the new protocol are 1076.2 +8.5/-8.8 ka and 944.7 +5.6/-5.6 ka respectively. The ^{238}U-^{234}U-^{206}Pb ages therefore replicate with an uncertainty of better than 1 %, irrespective of whether the matrix is removed or not. Moreover, the precision of the ages is not greatly degraded by applying the simplified protocol and interestingly, the higher analytical precision of the control data for the F layer does not translate to higher age precision because of scatter in the data.

^{238}U-^{234}U-^{206}Pb ages for SLL10-6 obtained using the new protocol vary systematically from 1076.2 +8.5/-8.8 ka near the stratigraphic base of the sample to 571.4 +13.7/-14.4 ka near the stratigraphic top of the sample, with no age reversals. Treating replicate and overlapping ages as single values, five distinct age values are observed. The likelihood of these ages falling in stratigraphic order as the consequence of a fluke result is, thus, 1 in 5!, or less than 1%.

^{235}U-^{207}Pb ages obtained for SLL10-6 using the new method are less precise than the ^{238}U-^{234}U-^{206}Pb ages owing mainly to the proportionally much larger common Pb correction on ^{207}Pb. Nevertheless, the most radiogenic analyses, layer G and F_{top} yield reasonable ^{235}U-^{207}Pb ages of 1060 +46/-48 ka and 960 +47/-54 ka respectively, in agreement with the corresponding ^{238}U-^{234}U-^{206}Pb ages of 1076.2 +8.5/-8.8 ka and 944.7 +5.6/-5.6 ka. All other obtained ^{235}U-^{207}Pb ages are also concordant with their corresponding ^{238}U-^{234}U-^{206}Pb ages.

5.3 JOHO-1

Results for JOHO-1 are given in Table 2 and Fig. 5. The results are intended as an inter-laboratory comparison of isotopic measurements made using the new protocol at the University of Oxford, with those obtained independently at NIGL by laser ablation. Results are given in terms of ^{238}U/^{206}Pb-^{207}Pb/^{206}Pb ratios for compatibility with the NIGL laser ablation measurements. In terms of the measured ^{238}U/^{206}Pb ratio, the precision of the two data sets is comparable (with typical ± 2 % uncertainties for the Oxford solution data versus ± 3% for the NIGL data; Table 2). However, the NIGL data targeted a small domain with up to 25 ppm U, whereas the solution measurements were made on material with a bulk U concentration of 0.3-0.5 ppm.

The NIGL data define a mixing trend from highly radiogenic compositions (with a ^{238}U/^{206}Pb ratio of c. 340 and a ^{207}Pb/^{206}Pb ratio of c. 0.05) falling just above concordia, towards a common Pb ^{207}Pb/^{206}Pb ratio of c. 0.65, but with the majority of the analyses clustering towards the radiogenic end of the trend. The Oxford data fall towards the radiogenic end of the same trend and are thus consistent with the NIGL analyses and yield a comparable age if common assumptions are used. Thus, for example, regression of each data set through a common ^{207}Pb/^{206}Pb ratio of 0.65 ± 0.1 yields concordia intercepts at 19.34 ± 0.30 Ma and 19.19 ± 0.15 Ma respectively for the Oxford solution data and NIGL laser ablation data (concordia assumes no initial ^{230}Th or ^{231}Pa and equilibrium initial ^{234}U and ^{226}Ra). Less spread towards unradiogenic compositions is seen in the Oxford data, but this is unsurprising given that fewer analyses were made.

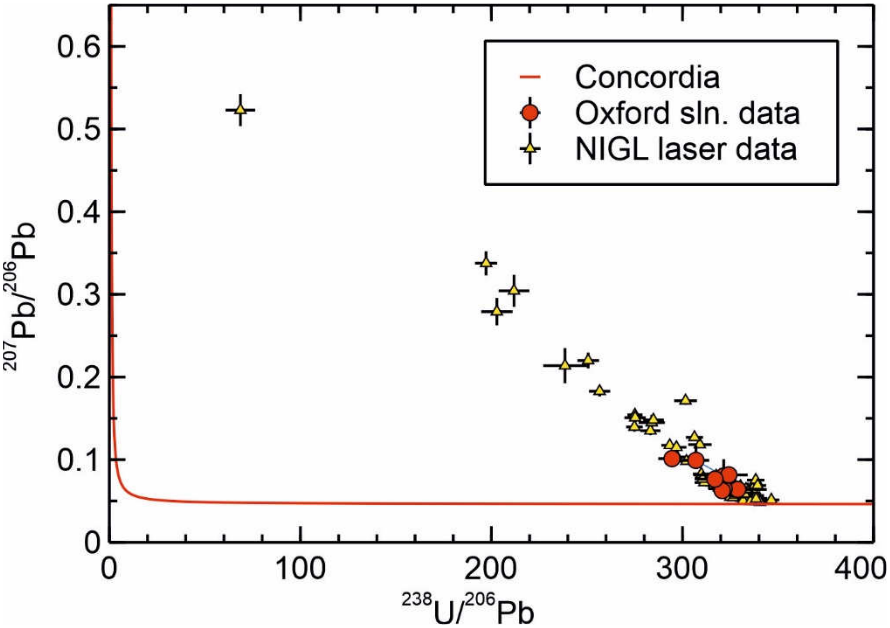

Figure 5: Tera-Wasserburg diagram showing a comparison of data from sample JOHO-1 obtained at NIGL by LA ICP-MS with data obtained at Oxford using the new method. Data are presented in $^{238}U/^{206}Pb$ – $^{207}Pb/^{206}Pb$ isotope space for compatibility with the NIGL LA data and because no independent measurement of the $^{232}Th/^{238}U$ is presently available. Equilibrium concordia is shown for reference. The co-linearity of the Oxford and NIGL data indicate the consistency of the two data sets. The intersection of the array of data with concordia at $^{238}U/^{206}Pb$ c. 340 and $^{207}Pb/^{206}Pb$ c. 0.05 gives the radiogenic end member without the use of a purely unradiogenic Pb isotope, but at the expense of obtaining independent $^{235}U/^{207}Pb$ ages. The intersection with concordia corresponds to an age of c. 19.25 Ma, assuming equilibrium initial ^{234}U. The intersection with the $^{207}Pb/^{206}Pb$ axis gives a common $^{207}Pb/^{206}Pb$ ratio of c. 0.65. The somewhat low (radiogenic) common $^{207}Pb/^{206}Pb$ ratio is attributed to ingrowth of ^{206}Pb in the source of the common Pb prior to sample formation.

6 SB_pk142 results

Results for SB_pk142 from Botovskaya cave are shown in Table 2 and Fig. 6. On a $^{208}Pb/^{206}Pb$-$^{238}U/^{206}Pb$ plot data from SB_pk142 fall on two distinct trends corresponding to the stratigraphically older and younger sections of the sample. The stratigraphically older part of the sample has a consistently lower $^{238}U/^{206}Pb$ ratio for a given $^{208}Pb/^{206}Pb$ ratio than the stratigraphically younger section. The intercept $^{238}U/^{206}Pb$ values of the two trends at c. 685 and c. 910, respectively for the older and younger sections of the sample correspond to apparent ^{238}U-^{206}Pb ages of c. 9.5 Ma and 7.2 Ma, assuming equilibrium initial ^{234}U and no initial ^{230}Th. The assumption that initial ^{234}U was in equilibrium is likely incorrect (see below) but demonstrates the point that there is an appreciable apparent age difference between the older and younger sections of the sample, which appears consistent with the apparent hiatus, and the age order superficially agrees with the stratigraphy of the sample. The common $^{208}Pb/^{206}Pb$ ratio suggested by the upper and lower sections of the sample are not appreciably different.

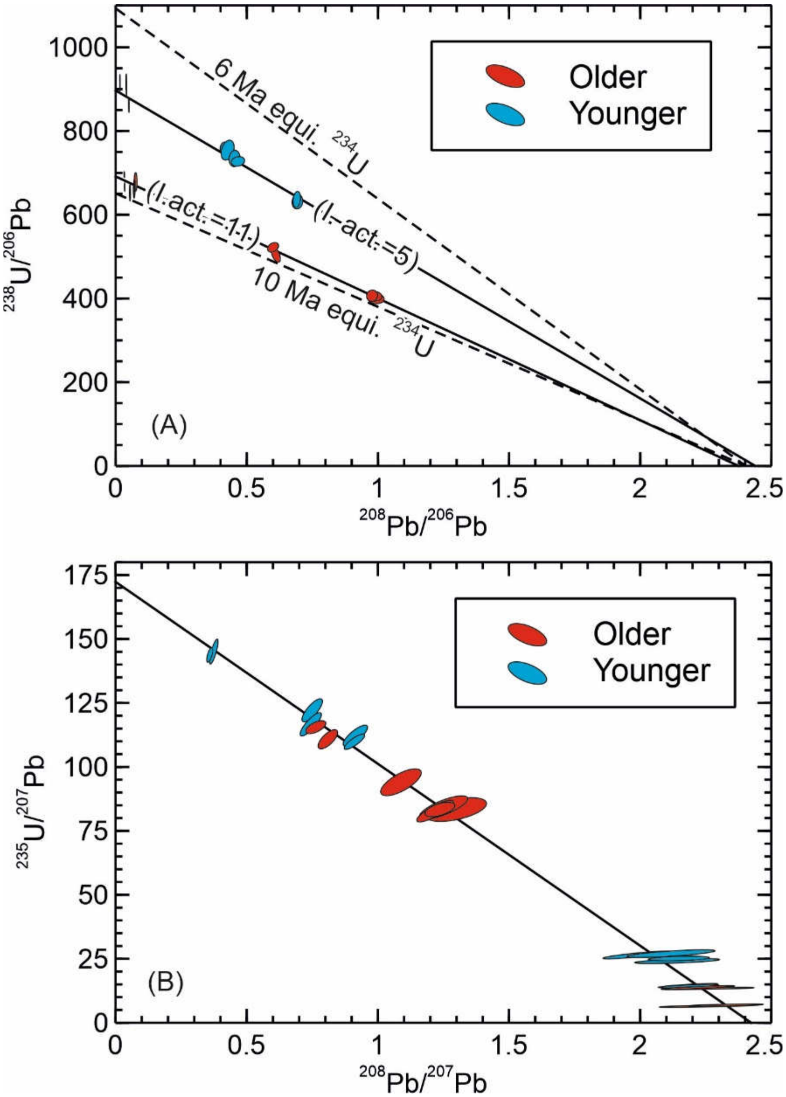

Figure 6: Isochron plots for sample SB_pk142. The 'older' and 'younger' sections are respectively stratigraphically older and younger than an iron oxide-stained lamina possibly marking a hiatus. Based on the maximum ^{232}Th/^{238}U observed for aragonite samples in this cave (Vaks et al., 2013a), ingrown ^{208}Pb is estimated to make no more than a c. 3 ‰ contribution to the ^{208}Pb/^{206}Pb and ^{208}Pb/^{207}Pb ratios for the most radiogenic analyses, becoming inconsequential for the least radiogenic analyses. This contribution is negligible for the common Pb correction and has a maximum effect on the (^{235}U-^{207}Pb) age of ~0.5 ‰. In both plots the isochron intersection with the x-axis corresponds to the common Pb composition, while in the effective absence of ingrown ^{208}Pb, the intersection with the y-axis corresponds to the ^{23y}U/^{20x}Pb$_{rad}$ ratio. A) ^{208}Pb/^{206}Pb-^{238}U/^{206}Pb plot showing the two portions of the sample falling on clearly distinct trends corresponding to apparent ^{238}U -^{206}Pb ages of c. 7.2 Ma and c. 9.5 Ma. The dashed lines are reference isochrons for 6 Ma and 10 Ma assuming equilibrium initial ^{234}U. The figures in brackets are the initial ^{234}U/^{238}U activity ratios associated with each portion of the sample, estimated by solving the ^{238}U-^{206}Pb decay equation using the ^{235}U-^{207}Pb age. B) ^{208}Pb/^{207}Pb-^{235}U/^{207}Pb plot showing the two sections of the sample falling on a common trend, suggesting they actually have a similar age of c. 6 Ma. The 6 Ma reference isochron on Fig. 6A is considered to represent the true age of the sample based on the ^{235}U-^{207}Pb data. The plotting of the data on two separate and apparently older isochrons in Fig. 6A is attributable to the distinct and high initial ^{234}U/^{238}U ratios in the two parts of the sample, which resulted in two populations of data with different radiogenic ^{206}Pb excesses relative to the 6 Ma reference isochron.

On a ^{208}Pb/^{207}Pb-^{235}U/^{207}Pb plot data from SB_pk142 show a rather different pattern and the data from both the stratigraphically older and younger portions of the sample define a single trend with an intercept of c. 171.2. This corresponds to a ^{235}U/^{207}Pb age of c. 6 Ma, and suggests the stratigraphically older and younger portions of the sample are not, in fact, appreciably different in age, and that the sample is rather younger than the ^{238}U-^{206}Pb system suggests.

The data show basically coherent mixing lines between a radiogenic end-member and common Pb. Thus, the discrepancy between the ^{238}U-^{206}Pb system and ^{235}U-^{207}Pb system cannot be easily attributed to open system behaviour. Moreover, such an explanation would require U or Pb isotopes from the two systems to have behaved differently. Extreme ^{234}U disequilibrium is, however, known to occur in samples from Botovskaya cave, with initial ^{234}U/^{238}U ratios between 3.4 and 8.1 times equilibrium reported for samples from the last 0.5 Ma based on U/Th dating (Vaks et al., 2013b, 2020). Excess ^{206}Pb from the decay of excess initial ^{234}U will make the ^{238}U/^{206}Pb$_{rad}$ ratio appear low (old) compared to the corresponding ^{235}U/^{207}Pb$_{rad}$ ratio, with the discrepancy depending on the initial ^{234}U/^{238}U ratio; in other words it allows time-independent variation of the ^{238}U/^{206}Pb$_{rad}$ ratio not seen in the ^{235}U/^{207}Pb ratio. This could account for older apparent ^{238}U-^{206}Pb ages and the difference between the ^{208}Pb/^{206}Pb-^{238}U/^{206}Pb and ^{208}Pb/^{207}Pb-^{235}U/^{207}Pb plots. Excluding subsamples 15-17, which are unradiogenic, the upper section of the sample gives a mean ^{235}U-^{207}Pb model age of 5.9 Ma with typical uncertainties on individual ^{235}U/^{207}Pb model ages of ± 0.2 to 0.3 Ma, and suggests an initial ^{234}U/^{238}U ratio varying between 3.8 and 5.8 times equilibrium (Table 2). This initial ^{234}U/^{238}U is typical of that already documented from Botovskaya cave. The lower section of the sample is generally slightly less radiogenic, but where subsamples yield ^{235}U/^{207}Pb ages they are indistinguishable from the upper section of the sample. Calculated initial ^{234}U/^{238}U ratios for the lower part of the sample are higher than those previously reported but not particularly unexpected for this cave, at between 10 and 11.6 times equilibrium. It is uncertain why the initial ^{234}U/^{238}U changed between the two sections of the sample, though the fact that a prominent iron oxide-stained lamina separates the two portions of the sample seems to indicate a change in growth conditions occurred.

Table 2. U-Pb data and ages

Table 2a. Preliminary test data for ASH-15 obtained without preconcentration of U and Pb.

	^{238}U/^{206}Pb	**+**	**-**	**^{208}Pb/^{206}Pb**	**+**	**-**
ASH-15I_1	1045	31	31	1.067	0.032	0.032
ASH-15I _1 (replicate)	1083	32	32	1.054	0.032	0.032
ASH-15I _2	1289	39	39	0.864	0.026	0.026
ASH-15I _3	1280	38	38	0.865	0.026	0.026
ASH-15I _4	1340	40	40	0.826	0.025	0.025
ASH-15I _5	1134	34	34	1.049	0.031	0.031
ASH-15I _5 (replicate)	1094	33	33	1.047	0.031	0.031

Uncertainties are 95% confidence

Table 2b. Isochron reference data for SLL10-6 F and G obtained with preconcentration of U and Pb. Each analysis is a separate subsample.

ID	**^{238}U/ ^{206}Pb**	**+**	**-**	**^{207}Pb/ ^{206}Pb**	**+**	**-**	**ρ (^{238}U/ ^{206}Pb- ^{207}Pb/ ^{206}Pb)^{a}**	**^{208}Pb/ ^{206}Pb**	**+**	**-**	**ρ (^{238}U/ ^{206}Pb- ^{208}Pb/ ^{206}Pb)^{a}**
SLL10-F-top	5328	4	3	0.03813	0.00069	0.00074	-0.71	0.0095	0.0012	0.0012	-0.72
SLL10-F-top	5325	5	4	0.03724	0.00100	0.00109	-0.84	0.0072	0.0018	0.0019	-0.85
SLL10-F-top	5337	4	5	0.03606	0.00100	0.00095	-0.79	0.0051	0.0017	0.0016	-0.80
SLL10-F-top	5320	3	3	0.03838	0.00053	0.00059	-0.63	0.0107	0.0010	0.0010	-0.64
SLL10-F-top	5286	4	4	0.04010	0.00098	0.00100	-0.81	0.0150	0.0018	0.0016	-0.82
SLL10-6-G	4720	40	34	0.07089	0.00519	0.00613	-0.95	0.0884	0.0131	0.0150	-0.98
SLL10-6-G	4564	30	26	0.08938	0.00397	0.00475	-0.95	0.1347	0.0100	0.0113	-0.97
SLL10-6-G	4910	46	40	0.04604	0.00610	0.00695	-0.96	0.0245	0.0154	0.0168	-0.98
SLL10-6-G	4915	49	42	0.04927	0.00643	0.00737	-0.96	0.0328	0.0163	0.0181	-0.98
SLL10-6-G	4872	39	32	0.05525	0.00488	0.00579	-0.96	0.0484	0.0123	0.0141	-0.98

Table 2b continued.

ID	**^{235}U/ ^{207}Pb**	**+**	**-**	**^{208}Pb/ ^{207}Pb**	**+**	**-**	**ρ (^{235}U/ ^{207}Pb-^{208}Pb/ ^{207}Pb)^{a}**	**^{234}U/ ^{238}U**	**+**	**-**
SLL10-F-top	1002	20	19	0.249	0.027	0.028	-0.93	5.9241E-05	7.0E-08	6.2E-08
SLL10-F-top	1026	32	28	0.194	0.042	0.046	-0.96	5.9223E-05	6.6E-08	6.7E-08
SLL10-F-top	1061	29	29	0.140	0.044	0.043	-0.96	5.9202E-05	6.6E-08	6.4E-08
SLL10-F-top	994	16	14	0.278	0.022	0.021	-0.91	5.9192E-05	5.9E-08	5.9E-08
SLL10-F-top	945	25	24	0.373	0.034	0.034	-0.94	5.9187E-05	6.0E-08	5.7E-08
Mean								5.9209E-05	2.8E-08	2.8E-08
SLL10-6-G	484	49	37	1.246	0.090	0.118	-0.93	5.7588E-05	6.5E-08	8.9E-08
SLL10-6-G	371	23	18	1.507	0.044	0.058	-0.88	5.7587E-05	6.0E-08	8.5E-08
SLL10-6-G	778	142	100	0.523	0.241	0.329	-0.97	5.7610E-05	5.7E-08	9.0E-08
SLL10-6-G	727	132	92	0.659	0.222	0.308	-0.97	5.7548E-05	6.2E-08	8.5E-08
SLL10-6-G	642	79	57	0.873	0.138	0.185	-0.96	5.7535E-05	6.2E-08	8.5E-08
Mean								5.7574E-05	3.9E-08	3.9E-08

Uncertainties are empirical 95% confidence Monte Carlo errors. The slight variations in the model values for different samples are random fluctuations arising from the Monte Carlo approach. Data are corrected for procedural blank.

[a] Correlation coefficient for the uncertainties on the specified ratio pairs.

Table 2c. U-Pb data, ^{238}U-^{234}U-^{206}Pb ages and ^{235}U-^{207}Pb ages for SLL10-6 obtained without preconcentration of U and Pb.

ID	**^{238}U/ ^{206}Pb**	**+**	**-**	**^{234}U/ ^{206}Pb**	**+**	**-**	**^{208}Pb/ ^{206}Pb**	**+**	**-**	**ρ (^{238}U/ ^{206}Pb- ^{208}Pb/ ^{206}Pb)^{a}**	**ρ (^{234}U/ ^{206}Pb- ^{208}Pb/ ^{206}Pb)^{a}**
SLL10-6 A	5741	65	71	0.3839	0.0043	0.0049	0.5001	0.0044	0.0045	-0.21	-0.21
SLL10-6 A	5777	97	96	0.3863	0.0065	0.0064	0.4987	0.0096	0.0093	0.07	0.07
SLL10-6 B	2047	169	158	0.1279	0.0106	0.0099	1.0315	0.0557	0.0547	-0.05	-0.05
SLL10-6 B	2054	146	133	0.1284	0.0091	0.0083	1.0144	0.0439	0.0436	-0.04	-0.04
SLL10-6 B re-cleaned	4156	71	73	0.2596	0.0045	0.0046	0.4725	0.0139	0.0119	0.14	0.14
SLL10-6 B re-cleaned	4175	75	92	0.2608	0.0047	0.0057	0.4664	0.0132	0.0106	-0.11	-0.11
SLL10-6 B-C hiatus	1441	35	67	0.0901	0.0022	0.0042	1.1233	0.0100	0.0090	-0.40	-0.40
SLL10-6 C	5546	116	110	0.3480	0.0074	0.0069	0.1473	0.0052	0.0028	0.04	0.04
SLL10-6 C	5509	60	59	0.3457	0.0038	0.0037	0.1479	0.0027	0.0018	-0.05	-0.05
SLL10-6 D re-cleaned	4561	129	172	0.2788	0.0080	0.0106	0.2768	0.0074	0.0073	-0.13	-0.13
SLL10-6 D re-cleaned	4585	96	108	0.2803	0.0058	0.0066	0.2723	0.0088	0.0060	0.16	0.16
SLL10-6 D-E hiatus	4683	44	39	0.2870	0.0027	0.0024	0.2345	0.0096	0.0056	0.06	0.06
SLL10-6 E	4324	74	112	0.2639	0.0045	0.0068	0.3369	0.0067	0.0057	-0.30	-0.30
SLL10-6 E	4315	72	82	0.2633	0.0044	0.0051	0.3329	0.0048	0.0052	0.18	0.18
SLL10-6 F top	5165	45	44	0.3057	0.0026	0.0026	0.0712	0.0016	0.0015	0.21	0.20
SLL10-6 F bottom	4543	48	43	0.2699	0.0029	0.0026	0.2035	0.0028	0.0024	-0.16	-0.16
SLL10-6 G	4838	59	56	0.2782	0.0034	0.0032	0.0545	0.0019	0.0015	-0.01	-0.01

Table 2c continued.

ID	**^{234}U/ ^{238}U**	**+**	**-**	**Model com. ^{208}Pb/ ^{206}Pb^{b}**	**+**	**-**	**^{238}U- ^{234}U- ^{206}Pb age (Ma)**	**+**	**-**
SLL10-6 A	6.6867E-05	1.3E-07	1.2E-07	1.471	0.100	0.102	0.5732	0.0130	0.0141
SLL10-6 A	6.6868E-05	1.3E-07	1.3E-07	1.470	0.098	0.096	0.5714	0.0137	0.0144
SLL10-6 B	6.2476E-05	5.8E-08	5.9E-08	1.470	0.100	0.096	0.7325	0.0907	0.1026
SLL10-6 B	6.2475E-05	5.7E-08	5.9E-08	1.472	0.098	0.101	0.7494	0.0791	0.0938
SLL10-6 B re-cleaned	6.2475E-05	6.0E-08	6.0E-08	1.470	0.099	0.099	0.7863	0.0177	0.0193
SLL10-6 B re-cleaned	6.2475E-05	6.0E-08	5.9E-08	1.471	0.100	0.101	0.7872	0.0186	0.0187
SLL10-6 B-C hiatus	6.2559E-05	5.3E-08	5.1E-08	1.471	0.100	0.100	0.7840	0.0927	0.1169
SLL10-6 C	6.2759E-05	5.7E-08	5.8E-08	1.471	0.100	0.099	0.7774	0.0099	0.0103
SLL10-6 C	6.2760E-05	5.9E-08	5.9E-08	1.470	0.097	0.103	0.7802	0.0062	0.0064
SLL10-6 D re-cleaned	6.1141E-05	5.8E-08	5.7E-08	1.470	0.099	0.100	0.8615	0.0199	0.0171
SLL10-6 D re-cleaned	6.1141E-05	5.6E-08	5.6E-08	1.472	0.101	0.101	0.8609	0.0149	0.0143
SLL10-6 D-E hiatus	6.1277E-05	5.1E-08	5.2E-08	1.471	0.098	0.098	0.8620	0.0081	0.0098
SLL10-6 E	6.1021E-05	5.7E-08	5.7E-08	1.470	0.102	0.097	0.8657	0.0153	0.0140
SLL10-6 E	6.1021E-05	5.7E-08	5.7E-08	1.471	0.102	0.100	0.8687	0.0146	0.0142
SLL10-6 F top	5.9194E-05	5.0E-08	4.9E-08	1.471	0.100	0.099	0.9447	0.0056	0.0056
SLL10-6 F bottom	5.9397E-05	5.0E-08	5.0E-08	1.470	0.101	0.100	0.9528	0.0081	0.0087
SLL10-6 G	5.7497E-05	4.8E-08	4.9E-08	1.471	0.099	0.102	1.0762	0.0085	0.0088

Table 2c continued.

ID	**Initial ^{234}U/ ^{238}U**	**+**	**-**	**^{235}U/ ^{207}Pb**	**+**	**-**	**^{208}Pb/ ^{207}Pb**	**+**	**-**	**ρ (^{235}U/ ^{207}Pb- ^{208}Pb/ ^{207}Pb)[a]**
SLL10-6 A	1.150E-04	2.2E-06	2.3E-06	186.7	2.9	2.9	2.240	0.059	0.044	0.72
SLL10-6 A	1.146E-04	2.4E-06	2.4E-06	183.4	4.6	4.6	2.180	0.079	0.079	0.74
SLL10-6 B	1.147E-04	1.7E-05	1.5E-05	32.5	3.8	4.0	2.255	0.363	0.315	0.76
SLL10-6 B	1.175E-04	1.5E-05	1.5E-05	34.6	4.2	3.4	2.355	0.340	0.306	0.82
SLL10-6 B re-cleaned	1.240E-04	3.5E-06	3.7E-06	143.3	4.0	3.9	2.244	0.121	0.091	0.79
SLL10-6 B re-cleaned	1.242E-04	3.7E-06	3.6E-06	140.8	4.7	6.4	2.167	0.075	0.099	0.58
SLL10-6 B-C hiatus	1.249E-04	2.0E-05	2.0E-05	22.2	0.7	0.7	2.390	0.073	0.057	0.27
SLL10-6 C	1.248E-04	2.0E-06	2.0E-06	453.7	12.3	12.5	1.661	0.061	0.059	0.55
SLL10-6 C	1.254E-04	1.3E-06	1.3E-06	439.8	14.2	17.2	1.626	0.082	0.068	0.91
SLL10-6 D re-cleaned	1.252E-04	4.1E-06	3.3E-06	239.1	9.4	10.2	2.000	0.101	0.103	0.57
SLL10-6 D re-cleaned	1.250E-04	3.0E-06	2.8E-06	242.8	7.1	10.6	1.988	0.080	0.103	0.72
SLL10-6 D-E hiatus	1.268E-04	1.7E-06	2.0E-06	283.8	4.3	3.7	1.957	0.094	0.057	0.29
SLL10-6 E	1.246E-04	3.1E-06	2.7E-06	191.4	5.1	5.5	2.055	0.093	0.085	0.74
SLL10-6 E	1.252E-04	2.9E-06	2.8E-06	195.3	5.6	5.5	2.076	0.080	0.068	0.83
SLL10-6 F top	1.157E-04	1.0E-06	9.7E-07	598.8	11.4	11.0	1.137	0.022	0.023	0.26
SLL10-6 F bottom	1.201E-04	1.5E-06	1.6E-06	288.5	5.0	5.5	1.780	0.039	0.035	0.56
SLL10-6 G	1.076E-04	1.3E-06	1.3E-06	614.3	8.8	9.1	0.953	0.034	0.028	0.33

Table 2c continued.

ID	**Model com. ^{208}Pb/ ^{207}Pb[b]**	**+**	**-**	**Model ^{238}U/ ^{235}U**	**+**	**-**	**^{207}Pb- ^{235}U age (Ma)**	**+**	**-**	**^{207}Pb/ ^{206}Pb**	**+**	**-**
SLL10-6 A	2.463	0.137	0.136	137.75	0.19	0.20				0.2233	0.0043	0.0046
SLL10-6 A	2.465	0.136	0.136	137.75	0.20	0.20	0.683	0.327	0.343	0.2288	0.0062	0.0063
SLL10-6 B	2.463	0.138	0.137	137.75	0.20	0.20				0.4592	0.0681	0.0609
SLL10-6 B	2.465	0.135	0.133	137.75	0.20	0.21				0.4325	0.0577	0.0536
SLL10-6 B re-cleaned	2.467	0.135	0.140	137.75	0.20	0.20				0.2105	0.0068	0.0067
SLL10-6 B re-cleaned	2.464	0.131	0.134	137.75	0.20	0.20	0.916	0.424	0.429	0.2153	0.0074	0.0060
SLL10-6 B-C hiatus	2.463	0.136	0.129	137.75	0.20	0.20				0.4700	0.0108	0.0132
SLL10-6 C	2.466	0.137	0.137	137.75	0.20	0.20	0.776	0.105	0.108	0.0887	0.0031	0.0030
SLL10-6 C	2.464	0.134	0.134	137.75	0.20	0.20	0.832	0.126	0.129	0.0910	0.0037	0.0031
SLL10-6 D re-cleaned	2.466	0.138	0.135	137.75	0.20	0.20	0.849	0.272	0.275	0.1385	0.0062	0.0055
SLL10-6 D re-cleaned	2.463	0.140	0.133	137.75	0.20	0.20	0.854	0.281	0.256	0.1371	0.0062	0.0051
SLL10-6 D-E hiatus	2.465	0.132	0.134	137.75	0.20	0.20	0.782	0.178	0.221	0.1198	0.0024	0.0024
SLL10-6 E	2.466	0.136	0.139	137.75	0.20	0.20	0.929	0.319	0.338	0.1640	0.0062	0.0056
SLL10-6 E	2.465	0.132	0.133	137.75	0.20	0.19	0.865	0.298	0.318	0.1604	0.0057	0.0053
SLL10-6 F top	2.466	0.132	0.143	137.75	0.20	0.20	0.960	0.047	0.054	0.0626	0.0013	0.0010
SLL10-6 F bottom	2.465	0.133	0.132	137.75	0.20	0.20	1.024	0.147	0.160	0.1143	0.0020	0.0022
SLL10-6 G	2.464	0.137	0.138	137.75	0.20	0.20	1.060	0.046	0.048	0.0572	0.0010	0.0010

Table 2c continued.

ID	**ρ (^{238}U/^{206}Pb-^{207}Pb/^{206}Pb)[a]**	**ρ (^{234}U/^{206}Pb-^{207}Pb/^{206}Pb)[a]**	**ρ (^{207}Pb/^{206}Pb-^{208}Pb/^{206}Pb)[a]**	**% concord-ance (^{235}U-^{207}Pb age/^{238}U-^{206}Pb age)**	**+**	**-**
SLL10-6 A	0.66	0.65	-0.08	-		
SLL10-6 A	0.42	0.42	-0.21	119.5	57.4	60.1
SLL10-6 B	0.50	0.50	0.05	-		
SLL10-6 B	0.49	0.49	-0.03	-		
SLL10-6 B re-cleaned	0.53	0.53	-0.20	-		
SLL10-6 B re-cleaned	-0.03	-0.03	0.15	116.3	53.1	54.0
SLL10-6 B-C hiatus	0.52	0.52	-0.19	-		
SLL10-6 C	0.58	0.58	0.30	99.9	13.8	14.4
SLL10-6 C	0.29	0.29	-0.09	106.6	16.3	16.6
SLL10-6 D re-cleaned	0.40	0.40	-0.09	98.5	31.8	32.0
SLL10-6 D re-cleaned	0.44	0.44	0.15	99.3	32.4	30.1
SLL10-6 D-E hiatus	0.69	0.69	0.12	90.7	20.6	25.4
SLL10-6 E	0.65	0.65	-0.34	107.4	37.3	39.3
SLL10-6 E	0.46	0.46	0.06	99.6	34.2	36.9
SLL10-6 F top	0.32	0.31	0.60	101.7	5.1	5.7
SLL10-6 F bottom	0.44	0.44	0.18	107.5	15.7	16.7
SLL10-6 G	0.59	0.59	0.06	98.5	4.5	4.6

Uncertainties are empirical 95% confidence Monte Carlo errors. The slight variations in the model values for different samples are random fluctuations arising from the Monte Carlo approach. Analyses with the same designation are replicate measurements of the same subsample.

[a] Correlation coefficient for the uncertainties on the specified ratio pairs.

[b] The assumed composition and uncertainty used to make corrections for the Pb initially in the samples.

Table 2d. U-Pb data obtained without preconcentration of U and Pb, ^{238}U-^{206}Pb reference ages and ^{235}U-^{207}Pb ages for SB_PK_142. The ^{238}U-^{206}Pb reference ages use an arbitrary assumed initial ^{234}U/^{238}U and are included only to highlight the apparent age difference between the upper and lower portion of the sample.

ID	**^{238}U/ ^{206}Pb**	**+**	**-**	**^{208}Pb/ ^{206}Pb**	**+**	**-**	**ρ (^{238}U/ ^{206}Pb- ^{208}Pb/ ^{206}Pb)[a]**	**Model initial ^{234}U/ ^{238}U[c]**	**+**	**-**
Subsamples 15-21 (stratigraphically younger than Fe stained lamina)										
SB_PK 142 (15)	630.5	14.3	14.2	0.6932	0.0186	0.0150	0.07	5.4999E-05	5.58E-08	5.37E-08
SB_PK 142 (15)	635.6	11.9	19.1	0.6912	0.0120	0.0113	0.19	5.5000E-05	5.38E-08	5.37E-08
SB_PK 142 (16)	726.7	8.4	10.3	0.4666	0.0276	0.0134	0.16	5.5000E-05	5.51E-08	5.53E-08
SB_PK 142 (16)	733.8	15.0	16.3	0.4535	0.0187	0.0150	0.10	5.5000E-05	5.66E-08	5.54E-08
SB_PK 142 (17)	753.5	17.4	21.3	0.4269	0.0274	0.0128	0.30	5.5000E-05	5.57E-08	5.30E-08
SB_PK 142 (17)	759.6	11.3	10.3	0.4118	0.0122	0.0091	0.25	5.5000E-05	5.42E-08	5.40E-08
SB_PK 142 (18)	851.3	6.7	6.5	0.0512	0.0009	0.0008	-0.17	5.5000E-05	5.60E-08	5.69E-08
SB_PK 142 (18)	860.5	14.7	13.4	0.0509	0.0010	0.0010	-0.11	5.5000E-05	5.41E-08	5.51E-08
SB_PK 142 (19)	897.4	16.3	16.1	0.0415	0.0007	0.0007	-0.06	5.5000E-05	5.54E-08	5.38E-08
SB_PK 142 (19)	917.2	16.0	15.7	0.0409	0.0010	0.0008	0.02	5.5000E-05	5.42E-08	5.50E-08
SB_PK 142 (20)	922.1	10.2	10.5	0.0167	0.0002	0.0003	0.03	5.5000E-05	5.65E-08	5.45E-08
SB_PK 142 (20)	906.5	10.9	10.8	0.0169	0.0003	0.0003	0.09	5.4999E-05	5.52E-08	5.47E-08
Subsamples 1-14 (stratigraphically older than Fe stained lamina)										
SB_PK 142 (1)	406.2	9.4	12.7	0.9789	0.0178	0.0165	0.07	5.5000E-05	5.46E-08	5.55E-08
SB_PK 142 (1)	404.8	9.1	9.0	0.9905	0.0223	0.0195	-0.05	5.5000E-05	5.50E-08	5.41E-08
SB_PK 142 (1)	399.1	9.8	9.4	0.9941	0.0277	0.0225	-0.05	5.5000E-05	5.56E-08	5.62E-08
SB_PK 142 (2)	677.8	18.2	18.0	0.0765	0.0049	0.0035	0.02	5.5001E-05	5.38E-08	5.45E-08
SB_PK 142 (2)	665.7	15.2	15.0	0.0720	0.0024	0.0021	0.04	5.5001E-05	5.38E-08	5.37E-08
SB_PK 142 (3)	656.2	14.4	13.9	0.0705	0.0017	0.0019	-0.14	5.5000E-05	5.55E-08	5.59E-08
SB_PK 142 (3)	664.4	11.2	10.9	0.0710	0.0013	0.0012	0.01	5.5000E-05	5.59E-08	5.53E-08
SB_PK 142 (4)	504.1	11.7	17.5	0.6115	0.0143	0.0143	-0.55	5.5000E-05	5.53E-08	5.43E-08
SB_PK 142 (4)	521.9	9.7	9.2	0.6011	0.0225	0.0113	0.31	5.5000E-05	5.50E-08	5.55E-08
SB_PK 142 (5)	695.3	5.7	6.5	0.0334	0.0011	0.0009	-0.35	5.5001E-05	5.34E-08	5.48E-08
SB_PK 142 (5)	665.5	9.0	8.5	0.0353	0.0007	0.0007	-0.13	5.5000E-05	5.63E-08	5.39E-08
SB_PK 142 (7)	652.0	16.3	15.8	0.0548	0.0017	0.0017	-0.06	5.4999E-05	5.47E-08	5.48E-08

Table 2d continued.

ID	**Model com. ^{208}Pb/ ^{206}Pb^{b}**	**+**	**-**	**^{238}U-^{206}Pb age (Ma) (assumed initial ^{234}U/^{238}U)^{c}**	**+**	**-**	**^{235}U/ ^{207}Pb**	**+**	**-**	**^{208}Pb/ ^{207}Pb**	**+**	**-**
Subsamples 15-21 (stratigraphically younger than Fe stained lamina)												
SB_PK 142 (15)	2.369	0.139	0.139	7.33	0.25	0.26	14.4	0.5	0.5	2.184	0.092	0.095
SB_PK 142 (15)	2.370	0.138	0.143	7.29	0.28	0.24	14.6	0.7	0.6	2.181	0.099	0.086
SB_PK 142 (16)	2.368	0.142	0.144	7.23	0.17	0.18	24.2	0.7	0.8	2.140	0.174	0.089
SB_PK 142 (16)	2.369	0.140	0.137	7.21	0.22	0.19	25.2	1.0	0.5	2.146	0.095	0.094
SB_PK 142 (17)	2.371	0.139	0.138	7.12	0.23	0.23	27.1	1.2	1.2	2.116	0.124	0.149
SB_PK 142 (17)	2.371	0.135	0.138	7.12	0.14	0.16	26.6	1.1	1.3	1.991	0.090	0.125
SB_PK 142 (18)	2.371	0.138	0.145	7.51	0.06	0.06	109.7	2.7	2.2	0.909	0.031	0.033
SB_PK 142 (18)	2.369	0.137	0.138	7.43	0.12	0.12	112.1	3.5	3.1	0.913	0.039	0.036
SB_PK 142 (19)	2.373	0.138	0.141	7.16	0.13	0.13	116.5	3.6	3.8	0.743	0.030	0.035
SB_PK 142 (19)	2.371	0.142	0.138	7.01	0.12	0.12	122.0	3.7	3.6	0.748	0.032	0.031
SB_PK 142 (20)	2.369	0.141	0.142	7.05	0.08	0.08	143.6	2.4	2.1	0.358	0.008	0.009
SB_PK 142 (20)	2.371	0.145	0.138	7.17	0.08	0.08	144.9	3.8	4.1	0.373	0.014	0.012
Subsamples 1-14 (stratigraphically older than Fe stained lamina)												
SB_PK 142 (1)	2.372	0.140	0.139	9.42	0.49	0.48	7.0	0.2	0.4	2.321	0.127	0.118
SB_PK 142 (1)	2.372	0.140	0.138	9.37	0.46	0.47	6.8	0.3	0.2	2.284	0.091	0.092
SB_PK 142 (1)	2.370	0.142	0.142	9.47	0.46	0.50	6.6	0.4	0.4	2.263	0.153	0.161
SB_PK 142 (2)	2.371	0.138	0.141	9.31	0.25	0.24	83.3	4.3	3.2	1.296	0.099	0.093
SB_PK 142 (2)	2.372	0.144	0.138	9.49	0.21	0.21	84.6	3.4	3.3	1.260	0.071	0.063
SB_PK 142 (3)	2.370	0.140	0.142	9.63	0.21	0.21	82.8	2.9	2.6	1.225	0.055	0.054
SB_PK 142 (3)	2.370	0.143	0.143	9.51	0.16	0.16	82.7	3.2	3.6	1.217	0.052	0.062
SB_PK 142 (4)	2.370	0.137	0.137	9.59	0.35	0.29	13.5	0.4	0.3	2.256	0.168	0.124
SB_PK 142 (4)	2.371	0.139	0.142	9.32	0.26	0.29	14.1	0.4	0.4	2.242	0.106	0.084
SB_PK 142 (5)	2.370	0.140	0.138	9.24	0.08	0.07	115.4	1.8	2.3	0.762	0.041	0.021
SB_PK 142 (5)	2.370	0.139	0.137	9.64	0.12	0.13	110.7	3.2	2.8	0.808	0.037	0.023
SB_PK 142 (7)	2.368	0.139	0.139	9.76	0.24	0.24	93.9	4.5	4.1	1.087	0.067	0.058

Table 2d continued.

ID	**ρ (^{235}U/ ^{207}Pb-^{208}Pb/ ^{207}Pb)[a]**	**Model com. ^{208}Pb/ ^{207}Pb[b]**	**+**	**-**	**Model ^{238}U/ ^{235}U**	**+**	**-**	**^{207}Pb-^{235}U age (Ma)**	**+**	**-**
Subsamples 15-21 (stratigraphically younger than Fe stained lamina)										
SB_PK 142 (15)	0.68	2.429	0.038	0.037	137.75	0.20	0.20	7.12	3.11	3.02
SB_PK 142 (15)	0.83	2.429	0.038	0.038	137.75	0.20	0.20	7.14	2.92	3.15
SB_PK 142 (16)	0.62	2.429	0.038	0.038	137.75	0.19	0.20	5.05	1.78	3.20
SB_PK 142 (16)	0.33	2.429	0.037	0.039	137.75	0.20	0.20	4.73	1.72	1.72
SB_PK 142 (17)	0.75	2.429	0.038	0.037	137.75	0.20	0.20	4.90	2.60	2.05
SB_PK 142 (17)	0.87	2.429	0.037	0.038	137.75	0.20	0.20	6.93	2.41	1.74
SB_PK 142 (18)	0.84	2.429	0.037	0.038	137.75	0.20	0.20	5.83	0.24	0.25
SB_PK 142 (18)	0.79	2.429	0.038	0.038	137.75	0.20	0.20	5.69	0.29	0.31
SB_PK 142 (19)	0.84	2.429	0.038	0.038	137.75	0.20	0.20	6.08	0.32	0.26
SB_PK 142 (19)	0.78	2.429	0.038	0.038	137.75	0.20	0.20	5.79	0.26	0.27
SB_PK 142 (20)	0.69	2.429	0.037	0.037	137.75	0.21	0.20	6.06	0.11	0.12
SB_PK 142 (20)	0.82	2.429	0.039	0.037	137.75	0.20	0.20	5.96	0.20	0.19
Subsamples 1-14 (stratigraphically older than Fe stained lamina)										
SB_PK 142 (1)	0.81	2.429	0.037	0.037	137.75	0.20	0.20			
SB_PK 142 (1)	0.66	2.429	0.038	0.038	137.75	0.20	0.19			
SB_PK 142 (1)	0.86	2.429	0.038	0.037	137.75	0.20	0.20			
SB_PK 142 (2)	0.51	2.429	0.038	0.037	137.75	0.20	0.20	5.72	0.63	0.68
SB_PK 142 (2)	0.70	2.429	0.039	0.038	137.75	0.21	0.19	5.81	0.51	0.51
SB_PK 142 (3)	0.61	2.429	0.037	0.038	137.75	0.21	0.20	6.11	0.44	0.44
SB_PK 142 (3)	0.85	2.429	0.038	0.038	137.75	0.20	0.20	6.16	0.59	0.47
SB_PK 142 (4)	0.66	2.429	0.037	0.038	137.75	0.21	0.20			
SB_PK 142 (4)	0.79	2.429	0.038	0.038	137.75	0.20	0.21			
SB_PK 142 (5)	0.62	2.429	0.037	0.039	137.75	0.20	0.20	6.07	0.19	0.24
SB_PK 142 (5)	0.71	2.429	0.037	0.038	137.75	0.21	0.20	6.15	0.22	0.31
SB_PK 142 (7)	0.71	2.429	0.037	0.037	137.75	0.20	0.20	6.01	0.50	0.53

Table 2d continued.

ID	**^{207}Pb/ ^{206}Pb**	+	-	**Initial (^{234}U/ ^{238}U)**	+	-
Subsamples 15-21 (stratigraphically younger than Fe stained lamina)						
SB_PK 142 (15)	0.3175	0.0120	0.0127	1.6	8.7	8.8
SB_PK 142 (15)	0.3170	0.0098	0.0139	1.4	8.9	8.2
SB_PK 142 (16)	0.2181	0.0060	0.0059	7.2	8.8	5.1
SB_PK 142 (16)	0.2114	0.0063	0.0083	8.0	4.9	5.0
SB_PK 142 (17)	0.2022	0.0117	0.0123	7.3	6.3	7.4
SB_PK 142 (17)	0.2071	0.0102	0.0091	1.5	5.0	6.7
SB_PK 142 (18)	0.0564	0.0013	0.0015	5.8	0.7	0.7
SB_PK 142 (18)	0.0557	0.0018	0.0019	5.9	1.0	0.9
SB_PK 142 (19)	0.0559	0.0022	0.0020	4.1	0.9	1.0
SB_PK 142 (19)	0.0546	0.0019	0.0019	4.4	0.9	0.9
SB_PK 142 (20)	0.0466	0.0008	0.0008	3.8	0.4	0.4
SB_PK 142 (20)	0.0454	0.0013	0.0012	4.4	0.5	0.6
Subsamples 1-14 (stratigraphically older than Fe stained lamina)						
SB_PK 142 (1)	0.4219	0.0272	0.0218			
SB_PK 142 (1)	0.4339	0.0155	0.0180			
SB_PK 142 (1)	0.4399	0.0292	0.0292			
SB_PK 142 (2)	0.0591	0.0028	0.0032	11.1	2.2	2.1
SB_PK 142 (2)	0.0572	0.0026	0.0024	11.4	1.7	1.7
SB_PK 142 (3)	0.0576	0.0021	0.0020	10.9	1.4	1.5
SB_PK 142 (3)	0.0583	0.0027	0.0022	10.5	1.4	1.7
SB_PK 142 (4)	0.2712	0.0101	0.0146			
SB_PK 142 (4)	0.2682	0.0089	0.0083			
SB_PK 142 (5)	0.0438	0.0010	0.0010	10.0	0.9	0.6
SB_PK 142 (5)	0.0436	0.0011	0.0013	10.9	0.9	0.7
SB_PK 142 (7)	0.0504	0.0027	0.0026	11.6	1.8	1.8

Uncertainties are empirical 95% confidence Monte Carlo errors. The slight variations in the model values for different samples are random fluctuations arising from the Monte Carlo approach. Analyses with the same designation are replicate measurements of the same subsample.

[a] Correlation coefficient for the uncertainties on the specified ratio pairs.

[b] The assumed composition and uncertainty used to make corrections for the Pb initially in the samples.

[c] The initial ^{234}U/^{238}U ratio is arbitrarily chosen to allow ^{238}U/^{206}Pb ages to be calculated to show the apparent age differences between the different sections of SB_PK 142. The ^{238}U/^{206}Pb ages should not be taken as an accurate estimate of the true age. The assigned initial ^{234}U/^{238}U uncertainty assumes a normal distribution.

[d] The estimated initial ^{234}U/^{238}U ratio estimated from the ^{238}U/radiogenic^{206}Pb ratio using the ^{235}U-^{207}Pb age.

Table 2e. U-Pb data and ^{238}U-^{206}Pb reference ages for JOHO-1 obtained without preconcentration of U and Pb.

ID	**^{238}U/ ^{206}Pb**	+	-	**^{208}Pb/ ^{206}Pb**	+	-	**^{207}Pb/ ^{206}Pb**	+	-	**Model initial ^{234}U/ ^{238}U^{c}**	+	-
JOHO-1 311.0 (1)	294.6	5.2	7.2	0.1455	0.0046	0.0069	0.1013	0.0104	0.0064	5.50E-05	5.60E-06	5.17E-06
JOHO-1 311.0 (1)	307.0	6.9	7.0	0.1450	0.0082	0.0051	0.0992	0.0178	0.0066	5.51E-05	5.45E-06	5.55E-06
JOHO-1 311.0 (1)	297.0	7.0	6.1	0.1537	0.0143	0.0093	0.1495	0.4652	0.0557	5.50E-05	5.18E-06	5.30E-06
JOHO-1 311.0 (2)	321.6	5.5	6.2	0.0713	0.0231	0.0093	0.0801	0.0204	0.0074	5.49E-05	5.53E-06	5.66E-06
JOHO-1 311.0 (2)	325.2	8.9	7.2	0.0867	0.0317	0.0123	0.0664	0.0029	0.0027	5.51E-05	5.25E-06	5.68E-06
JOHO-1 311.0 (2)	324.3	4.0	4.3	0.0613	0.0069	0.0036	0.0701	0.0054	0.0044	5.49E-05	5.19E-06	5.60E-06
JOHO-1 311.0 (3)	328.9	15.1	7.2	0.0495	0.0028	0.0021	0.0640	0.0035	0.0037	5.50E-05	5.89E-06	5.62E-06
JOHO-1 311.0 (3)	321.8	7.0	8.2	0.0498	0.0027	0.0033	0.0647	0.0036	0.0027	5.51E-05	5.50E-06	5.13E-06
JOHO-1 311.0 (3)	320.8	5.3	5.0	0.0486	0.0020	0.0020	0.0626	0.0039	0.0026	5.49E-05	5.41E-06	5.05E-06
JOHO-1 311.0 (4)	338.0	9.9	9.5	0.0889	0.0050	0.0048	0.0874	0.0648	0.0096	5.52E-05	5.25E-06	5.21E-06
JOHO-1 311.0 (4)	324.3	9.8	18.5	0.0986	0.0055	0.0066	0.0816	0.0048	0.0068	5.50E-05	5.01E-06	4.78E-06
JOHO-1 311.0 (4)	317.0	8.8	8.7	0.0924	0.0096	0.0048	0.0764	0.0050	0.0038	5.50E-05	5.64E-06	5.35E-06

Table 2e continued.

ID	**Model com. ^{208}Pb/^{206}Pb**[b]	**+**	**-**	**^{238}U-^{206}Pb age (Ma) (assumed initial ^{234}U/^{238}U)**[c]	**+**	**-**	**ρ (^{238}U/^{206}Pb-^{208}Pb/^{206}Pb)**[a]
JOHO-1 311.0 (1)	2.20	0.53	0.49	20.50	0.56	0.54	-0.18
JOHO-1 311.0 (1)	2.20	0.50	0.48	19.68	0.54	0.59	0.21
JOHO-1 311.0 (1)	2.20	0.46	0.51	20.25	0.54	0.67	0.14
JOHO-1 311.0 (2)	2.19	0.49	0.49	19.46	0.39	0.42	-0.22
JOHO-1 311.0 (2)	2.20	0.48	0.48	19.11	0.51	0.57	-0.11
JOHO-1 311.0 (2)	2.20	0.48	0.53	19.40	0.30	0.28	-0.19
JOHO-1 311.0 (3)	2.20	0.49	0.51	19.23	0.44	0.86	-0.23
JOHO-1 311.0 (3)	2.18	0.50	0.54	19.65	0.50	0.44	-0.01
JOHO-1 311.0 (3)	2.21	0.50	0.48	19.73	0.35	0.35	0.29
JOHO-1 311.0 (4)	2.22	0.47	0.50	18.38	0.54	0.53	-0.35
JOHO-1 311.0 (4)	2.20	0.52	0.52	19.06	1.15	0.65	-0.17
JOHO-1 311.0 (4)	2.20	0.49	0.52	19.55	0.57	0.56	0.01

Uncertainties are empirical 95% confidence Monte Carlo errors. The slight variations in the model values for different samples are random fluctuations arising from the Monte Carlo approach.

[a] Correlation coefficient for the uncertainties on the specified ratio pairs.

[b] The assumed composition and uncertainty used to make corrections for the Pb initially in the samples.

[c] The initial ^{234}U/^{238}U ratio is arbitrarily chosen to allow ^{238}U/^{206}Pb ages to be calculated. In the absence of direct constraint of the initial ^{234}U/^{238}U ratio, these ages should be treated with caution. The assigned initial ^{234}U/^{238}U uncertainty assumes a normal distribution.

Table 2f. Reference laser ablation U-Pb data for JOHO-1.

Spot	**$^{238}U/^{206}Pb$**	**±**	**$^{207}Pb/^{206}Pb$**	**±**
JOHO-1_01	211.8	16.0	0.3043	0.0387
JOHO-1_02	202.8	16.4	0.2791	0.0328
JOHO-1_03	317.3	8.1	0.0682	0.0032
JOHO-1_04	274.9	8.6	0.1396	0.0111
JOHO-1_05	283.2	10.6	0.1350	0.0108
JOHO-1_06	319.6	12.0	0.0796	0.0059
JOHO-1_07	311.4	10.1	0.0724	0.0059
JOHO-1_08	283.9	13.6	0.1450	0.0183
JOHO-1_09	275.1	7.8	0.1542	0.0068
JOHO-1_10	301.6	11.8	0.1713	0.0094
JOHO-1_11	331.7	8.2	0.0505	0.0016
JOHO-1_12	333.1	8.2	0.0578	0.0019
JOHO-1_13	325.0	8.3	0.0549	0.0016
JOHO-1_14	284.8	10.8	0.1481	0.0118
JOHO-1_15	309.1	12.2	0.1183	0.0082
JOHO-1_16	318.1	9.9	0.0693	0.0041
JOHO-1_17	319.6	8.6	0.0716	0.0038
JOHO-1_18	316.7	9.6	0.0692	0.0039
JOHO-1_19	256.6	11.1	0.1828	0.0125
JOHO-1_20	275.2	11.2	0.1508	0.0113
JOHO-1_21	333.0	8.4	0.0592	0.0032
JOHO-1_22	338.4	7.4	0.0496	0.0014
JOHO-1_23	305.6	8.9	0.0987	0.0061
JOHO-1_24	322.6	8.5	0.0751	0.0042
JOHO-1_25	319.5	9.1	0.0796	0.0055
JOHO-1_26	309.9	8.8	0.0826	0.0059
JOHO-1_27	306.4	7.9	0.1006	0.0060
JOHO-1_28	293.3	8.9	0.1173	0.0094
JOHO-1_29	326.5	8.5	0.0542	0.0018
JOHO-1_30	296.8	10.5	0.1150	0.0082
JOHO-1_31	297.2	12.6	0.1032	0.0150
JOHO-1_32	310.5	8.3	0.0767	0.0031
JOHO-1_33	327.4	8.8	0.0574	0.0020
JOHO-1_34	340.3	8.0	0.0531	0.0017
JOHO-1_35	322.8	10.0	0.0800	0.0051
JOHO-1_36	328.5	8.9	0.0594	0.0023
JOHO-1_37	317.6	9.1	0.0803	0.0036
JOHO-1_38	319.5	8.5	0.0803	0.0046
JOHO-1_39	338.5	8.3	0.0566	0.0019
JOHO-1_40	302.1	9.8	0.0983	0.0058
JOHO-1_41	68.6	15.4	0.5229	0.0385
JOHO-1_42	318.3	9.5	0.0698	0.0037
JOHO-1_43	320.2	7.6	0.0627	0.0023
JOHO-1_44	238.5	22.8	0.2137	0.0424
JOHO-1_45	197.2	11.6	0.3376	0.0291
JOHO-1_46	336.6	8.4	0.0643	0.0036
JOHO-1_47	335.6	8.3	0.0497	0.0020
JOHO-1_48	332.5	8.0	0.0587	0.0027
JOHO-1_49	346.5	8.3	0.0513	0.0016
JOHO-1_50	334.3	8.7	0.0637	0.0035
JOHO-1_51	250.6	11.3	0.2200	0.0188
JOHO-1_52	330.4	8.5	0.0678	0.0032
JOHO-1_53	338.3	9.0	0.0754	0.0050
JOHO-1_54	319.7	9.0	0.0809	0.0037
JOHO-1_55	306.3	8.9	0.1270	0.0050
JOHO-1_56	339.3	8.9	0.0688	0.0026
JOHO-1_57	340.6	8.6	0.0487	0.0016
JOHO-1_58	338.5	8.8	0.0526	0.0017
JOHO-1_59	333.3	8.0	0.0645	0.0052
JOHO-1_60	322.3	8.6	0.0606	0.0027

Uncertainties are 2 sigma

7 Discussion

7.1 Method validation

The results from the samples used for method validation indicate that the new protocol passes all four method validation tests. This in turn implicitly demonstrates that matrix effects such as molecular interferences or decoupling of U and Pb mass fractionation during analysis are either unimportant or can be adequately controlled with proper setup of the instrument. Similarly, significant biases introduced during sample preparation, such as preferential leaching of U or Pb during partial sample dissolution by the spike, can also be excluded.

Not separating the matrix does not lead to inconsistent data in the preliminary test using ASH-15, that is to say the data with and without matrix separation are co-linear, i.e. they define a common isochron, and therefore would yield the same ^{238}U/^{206}Pb age. Replication of ^{238}U-^{234}U-^{206}Pb ages with and without matrix separation is demonstrated to a high precision for the F and G layers of SLL10-6, again demonstrating that matrix separation via anion exchange chemistry is not necessary for U/Pb measurements. This finding is in line with the fact that laser ablation techniques have allowed measurements for a number of years without matrix separation (e.g. Roberts et al., 2017).

For SLL10-6, ^{238}U-^{234}U-^{206}Pb ages obtained with the new protocol from all stratigraphic layers vary systematically with stratigraphic order, without age reversals. Moreover, for sample layers that are sufficiently radiogenic to allow ^{235}U-^{207}Pb ages to be calculated, these are concordant with the ^{238}U-^{234}U-^{206}Pb ages, demonstrating the ability of the new protocol to exploit the ^{235}U-^{207}Pb system where the nature of the sample permits, even on material as young as c. 1 Ma. This is significant because it demonstrates the ability to have a continuity of dating between young samples where the initial ^{234}U can be directly constrained via the ^{238}U-^{234}U-^{206}Pb chronometer and old material (i.e. >20 Ma) where ^{238}U-^{206}Pb age inaccuracies associated with assuming the initial ^{234}U/^{238}U ratio will be proportionally small compared to the age.

Analysis of JOHO-1 using the new protocol replicates independently obtained laser ablation data, demonstrating inter-laboratory consistency of the new method. Additional data quality tests of the new method are presented in the larger data set of Vaks et al. (2020) in the form of comparison with U-Th ages and the testing of age reproducibility between different speleothems from a single location.

7.2 ^{238}U-^{206}Pb Russian roulette and the utility of the ^{235}U-^{207}Pb system

One of the major limitations to applying the ^{238}U-^{206}Pb system to geologically young materials just beyond the limit of the ^{238}U-^{234}U-^{206}Pb chronometer (a few million years) is that while ages can be highly precise (e.g. Woodhead et al., 2006), an age calculated assuming equilibrium initial ^{234}U/^{238}U and one calculated using the most extreme known initial ^{234}U/^{238}U ratio differ by >2 Ma, which is proportionally a massive difference for ages of a few million years. While it is possible to try to characterise initial ^{234}U/^{238}U for a particular cave using younger material (e.g. Woodhead et al., 2006), it is difficult to test whether such younger material is representative, and in some instances, younger material may simply not exist. Consequently, ^{238}U-^{206}Pb dating beyond the limit of the ^{238}U-^{234}U-^{206}Pb chronometer is something of a game of Russian roulette in terms of age accuracy, with SB_pk142 from Botovskaya cave being an example of where the 'bullet' of extreme initial ^{234}U disequilibrium is in the chamber. The ^{235}U-^{207}Pb chronometer provides an alternative option for highly radiogenic samples. Moreover, because decay of excess ^{234}U leads to a permanent excess of radiogenic ^{206}Pb relative to radiogenic ^{207}Pb, comparison of the ^{238}U-^{206}Pb and ^{235}U-^{207}Pb systems can be used to constrain initial ^{234}U/^{238}U after any residual disequilibrium has decayed (e.g. Mason et al., 2013). This is potentially very useful for testing assumed initial ^{238}U/^{234}U ratios used for other samples in a set where these can only be dated by the ^{238}U-^{206}Pb chronometer, because of common Pb.

7.3 Applicability of the new protocol and potential future development

The present method is only applicable to samples in which ^{232}Th is near absent. The method is not intended as a blanket replacement for prior implementations of the U-Pb system, but rather as a complementary technique that can be applied where it is best suited.

The new protocol has significant advantages over a traditional solution-based approach in terms of the simplicity of sample preparation for U-Pb analysis. Sample preparation is fast to the point that prior reconnaissance characterisation of the U-Pb system is unnecessary as the time penalty for preparing an undatable sample is minimal. Moreover, redundant sample material can be prepared with little extra effort, such that an analytical session can be re-targeted on the fly, as it becomes apparent which material is most favourable for dating. The greatly reduced sample preparation also eliminates stages at which contamination could occur (column chemistry, sample dry-downs), reducing the need for an optimal lab/column setup. The more traditional solution-based approach with purification of U and Pb retains an advantage in terms of analytical precision (at least under ideal conditions, e.g. the SLL10-6 F control data; Table 2) and, therefore, is likely to remain the preferred approach for the calibration of reference materials (e.g. Roberts et al., 2017). However, high analytical precision may not translate to high age precision if other limiting factors, such as scatter in the data, are present (as in the SLL10-6 F control data; also see compilation of Woodhead and Petrus (2019)) – i.e., the lower analytical precision of the new procedure need not be a significant limitation in terms of age precision. Indeed, the utilisation of the new approach by us (Vaks et al., 2020) to obtain c. 50 ^{238}U-^{234}U-^{206}Pb ages, many with corresponding concordant ^{235}U-^{207}Pb ages, on material <1.6 Ma old, demonstrates that it can be applied effectively 'in the wild' to generate fairly large data sets. In this case, the reduction in analytical effort achieved with the new approach allowed replication of growth ages between different stalagmites, providing additional quality control that would not otherwise have been available.

The new protocol does not provide an alternative for *in situ* techniques where high spatial resolution is required, e.g. on samples that are very small or have a complex morphology (e.g. Li et al., 2014). However, the results from JOHO-1 indicate the new method can be applied to carbonates with <1 ppm U. Although not investigated in detail, the comparable precision of the JOHO-1 solution and laser ablation data, despite the latter being acquired on a domain with > 10 × the U concentration, suggests the new protocol would outperform laser ablation in terms of the lower U and Pb concentration limit at which ages could be obtained. Moreover, the higher precision $^{234}U/^{238}U$ measurements obtained with the new method relative to laser ablation (< ± 1 ‰ attained here versus ± 5-6 ‰ obtained by Lin et al. (2017) by laser ablation) makes the former generally more suitable for ^{238}U-^{234}U-^{206}Pb dating, where quantifying slight residual disequilibrium in the $^{234}U/^{238}U$ ratio can be critical.

The new protocol was developed on a first generation Nu plasma, an instrument c. 20 years old at the time of writing. Hardware advancements, notably the Isotopx ATONA amplifier, which can greatly expand the dynamic range of Faraday collectors in to the range traditionally that of the ion counter (Szymanowski and Schoene, 2020), offer future potential to refine the present methodology. While the small ^{206}Pb, ^{207}Pb, and ^{208}Pb signals from radiogenic samples would still likely require measurement on ion counters, with suitable spike design, it may be possible to shift measurement of the Pb spike isotope and also ^{202}Hg on to Faraday collectors, providing more flexibility in the collector configurations that could be used. In particular, it may be a means to measure ^{207}Pb simultaneously with the spike isotope to help improve the precision of the $^{235}U/^{207}Pb$ ratio. Similarly, it may be possible to avoid the use of ion counting for small ^{235}U signals, simplifying the analysis.

Demonstrating the ability to make U-Pb measurements by directly dissolving samples with an isotopic tracer, and analysing with no further preparation other than dilution, opens another intriguing possibility for future method development; the prospect of some form of quasi-*in situ* isotope dilution analysis. If an acid cleaned subsample can be dissolved directly with the tracer and analysed, there is no reason, in principle, why an entire sample could not be acid cleaned, and small domains then dissolved with the tracer for analysis while still *in situ*. Obviously, there would be practical hurdles to overcome, and this would not be a substitute for high spatial resolution techniques, but it could substantially streamline isotope dilution analysis and make it less destructive to the sample.

8 Conclusions

A new isotope dilution method for the U-Pb dating of carbonate samples is presented which removes the need for preconcentration of Pb. The new method produces data consistent with those obtained by isotope dilution with preconcentration of U and Pb, and with data obtained independently by another laboratory using laser ablation ICP-MS. The new method also generates self-consistent data; specifically, ages that vary systematically with growth direction without age reversals and which are concordant between the ^{238}U-^{234}U-^{206}Pb and the ^{235}U-^{207}Pb chronometers. The new method thus satisfies reasonable data quality control criteria.

The new method is capable of utilising both the ^{238}U-^{234}U-^{206}Pb chronometer and the ^{235}U-^{207}Pb chronometers, subject to inherent limitations imposed by sample age and isotopic composition.

Data Availability. All data used are contained within Table 2.

Author Contribution. AM carried out the isotope dilution method development, analyses, and age interpretation. AV, GH, and SB obtained funding supporting this work. AV, SB and JH obtained samples and assisted with sample preparation. JH provided reference laser ablation data. AM wrote the manuscript with input from all co-authors.

Competing interests. The authors declare that they have no conflict of interest.

Acknowledgements. NERC grants NE/K005057/1 and NE/G013829/1 and DFG grant BR 3437/3-1 are acknowledged for partially supporting the present work. Speleoclub Arabika Irkutsk is thanked for invaluable assistance in obtaining speleothem samples from Siberia. Dr Nick Roberts (NIGL) is thanked for assistance in obtaining reference laser ablation data for JOHO-1. Shell is thanked for providing sample JOHO-1. R. A. Cliff and R. B. Ickert are thanked for constructive reviews.

References

Bajo, P., Drysdale, R., Woodhead, J., Hellstrom, J. and Zanchetta, G.: High-resolution U-Pb dating of an Early Pleistocene stalagmite from Corchia Cave (central Italy), Quat. Geochronol., 14, 5–17, doi:10.1016/j.quageo.2012.10.005, 2012.

Belshaw, N. S., Freedman, P. A., O'Nions, R. K., Frank, M. and Guo, Y.: A new variable dispersion double-focusing plasma mass spectrometer with performance illustrated for Pb isotopes, Int. J. Mass Spectrom., 181, 51–58, 1998.

Cheng, H., Edwards, R. L., Murrell, M. T. and Benjamin, T. M.: Uranium-thorium-protactinium dating systematics, Geochim. Cosmochim. Acta, 62(21–22), 3437–3452, doi:10.1016/S0016-7037(98)00255-5, 1998.

Cheng, H., Lawrence Edwards, R., Shen, C. C., Polyak, V. J., Asmerom, Y., Woodhead, J., Hellstrom, J., Wang, Y., Kong, X., Spötl, C., Wang, X. and Calvin Alexander, E.: Improvements in ^{230}Th dating, ^{230}Th and ^{234}U half-life values, and U-Th isotopic measurements by multi-collector inductively coupled plasma mass spectrometry, Earth Planet. Sci. Lett., 371–372, 82–91, doi:10.1016/j.epsl.2013.04.006, 2013.

Cliff, R. A., Spötl, C. and Mangini, A.: U-Pb dating of speleothems from Spannagel Cave, Austrian Alps: A high resolution comparison with U-series ages, Quat. Geochronol., 5(4), 452–458, doi:10.1016/j.quageo.2009.12.002, 2010.

Edwards, R. L., Gallup, C. D. and Cheng, H.: Uranium-series Dating of Marine and Lacustrine Carbonates, Rev. Mineral. Geochemistry, 52(1), 363–405, doi:10.2113/0520363, 2003.

Faure, G.: Principles of Isotope Geology, John Wiley & Sons, New York, 1986.

Getty, S. R., Asmerom, Y., Quinn, T. M. and Budd, A. F.: Accelerated Pleistocene coral extinctions in the Caribbean Basin shown by uranium-lead (U-Pb) dating, Geology, 29(7), 639–642, doi:10.1130/0091-7613(2001)029<0639:APCEIT>2.0.CO;2, 2001.

Heaman, L. and Parrish, R.: U-Pb Geochrononology of Accessory Minerals, in Short course Handbook on Applications of Radiogenic Isotope Systems to Problems in Geology, edited by L. Heaman and J. N. Ludden, pp. 59–102, Mineralogical Association of Canada., 1991.

Hiess, J., Condon, D. J., McLean, N. and Noble, S. R.: ^{238}U/^{235}U Systematics in Terrestrial Uranium-Bearing Minerals, Science, 335(6076), 1610 LP – 1614, doi:10.1126/science.1215507, 2012.

Kronfeld, J., Vogel, J. C. and Talma, A. S.: A new explanation for extreme ^{234}U/^{238}U disequilibria in a dolomitic aquifer, Earth Planet. Sci. Lett., 123(1–3), 81–93, doi:10.1016/0012-821X(94)90259-3, 1994.

Li, Q., Parrish, R. R., Horstwood, M. S. A. and Mcarthur, J. M.: U – Pb dating of cements in Mesozoic ammonites, Chem. Geol., 376, 76–83, doi:10.1016/j.chemgeo.2014.03.020, 2014.

Lin, Y., Jochum, K. P., Scholz, D., Hoffmann, D. L., Stoll, B., Weis, U. and Andreae, M. O.: In-situ high spatial resolution LA-MC-ICPMS ^{230}Th/U dating enables detection of small-scale age inversions in speleothems, Solid Earth Sci., 2(1), 1–9, doi:10.1016/j.sesci.2016.12.003, 2017.

Ludwig, K. R.: Effect of initial radioactive-daughter disequilibrium on U-Pb isotope apparent ages of young minerals, J. Res., 5(6), 663–667, 1977.

Ludwig, K. R.: On the treatment of concordant uranium-lead ages, Geochim. Cosmochim. Acta, 62(4), 665–676, doi:10.1016/S0016-7037(98)00059-3, 1998.

Mason, A. J. and Henderson, G. M.: Correction of multi-collector-ICP-MS instrumental biases in high-precision uranium-thorium chronology, Int. J. Mass Spectrom., 295(1–2), 26–35, doi:10.1016/j.ijms.2010.06.016, 2010.

Mason, A. J., Henderson, G. M. and Vaks, A.: An acetic acid-based extraction protocol for the recovery of U, Th and Pb from calcium carbonates for U-(Th)-Pb geochronology, Geostand. Geoanalytical Res., 37(3), 261–275, doi:10.1111/j.1751-908X.2013.00219.x, 2013.

Moorbath, S., Taylor, P. N., Orpen, J. L., Treloar, P. and Wilson, J. F.: First direct radiometric dating of Archaean stromatolitic limestone, Nature, 326(6116), 865–867, doi:10.1038/326865a0, 1987.

Nuriel, P., Rosenbaum, G., Zhao, J.-X., Feng, Y., Golding, S. D., Villemant, B. and Weinberger, R.: U-Th dating of striated fault planes, Geology, 40(7), 647–650, doi:10.1130/G32970.1, 2012.

Pickering, R., Kramers, J. D., Partridge, T., Kodolanyi, J. and Pettke, T.: Quaternary Geochronology U – Pb dating of calcite – aragonite layers in speleothems from hominin sites in South Africa by MC-ICP-MS, Quat. Geochronol., 5(5), 544–558, doi:10.1016/j.quageo.2009.12.004, 2010.

Plagnes, V., Causse, C., Genty, D., Paterne, M. and Blamart, D.: A discontinuous climatic record from 187 to 74 ka from a speleothem of the Clamouse Cave (south of France), Earth Planet. Sci. Lett., 201(1), 87–103, doi:10.1016/S0012-821X(02)00674-X, 2002.

Rasbury, E. T. and Cole, J. M.: Directly dating geologic events: U-Pb dating of carbonates, Rev. Geophys., 47, 1–27, doi:10.1029/2007RG000246.1.INTRODUCTION, 2009.

Rasbury, E. T., Hanson, G. N., Meyers, W. J. and Saller, A. H.: Dating of the time of sedimentation using U□Pb ages for paleosol calcite, Geochim. Cosmochim. Acta, 61(7), 1525–1529, doi:https://doi.org/10.1016/S0016-7037(97)00043-4, 1997.

Richards, D. A., Bottrell, S. H., Cliff, R. A., Ströhle, K. and Rowe, P. J.: U-Pb dating of a speleothem of Quaternary age, Geochim. Cosmochim. Acta, 62(23), 3683–3688, 1998.

Roberts, N. M. W., Rasbury, E. T., Parrish, R. R., Smith, C. J., Horstwood, M. S. A. and Condon, D. J.: A calcite reference material for LA-ICP-MS U-Pb geochronology, Geochemistry, Geophys. Geosystems, 2807–2814, doi:10.1002/2016GC006784.Received, 2017.

Scholz, D. and Hoffmann, D.: ^{230}Th/U-dating of fossil corals and speleothems, E&G Quat. Sci. J., 57(1/2), 52–76, doi:10.3285/eg.57.1-2.3, 2008.

Spooner, P. T., Chen, T., Robinson, L. F. and Coath, C. D.: Rapid uranium-series age screening of carbonates by laser ablation mass spectrometry, Quat. Geochronol., 31, 28–39, doi:10.1016/j.quageo.2015.10.004, 2016.

Steiger, R. H. and Jäger, E.: Subcommission on geochronology: Convention on the use of decay constants in Geo- and Cosmochronology, Earth Planet. Sci. Lett., 36, 359–362, 1977.

Stirling, C. H., Andersen, M. B., Potter, E. K. and Halliday, A. N.: Low-temperature isotopic fractionation of uranium, Earth Planet. Sci. Lett., 264(1–2), 208–225, doi:10.1016/j.epsl.2007.09.019, 2007.

Szymanowski, D. and Schoene, B.: U-Pb ID-TIMS geochronology using ATONA amplifiers, J. Anal. At. Spectrom., 35(6), 1207–1216, doi:10.1039/d0ja00135j, 2020.

Thomas, A. L., Fujita, K., Iryu, Y., Bard, E., Cabioch, G., Camoin, G., Cole, J. E., Deschamps, P., Durand, N., Hamelin, B., Heindel, K., Henderson, G. M., Mason, A. J., Matsuda, H., Ménabréaz, L., Omori, A., Quinn, T., Sakai, S., Sato, T., Sugihara, K., Takahashi, Y., Thouveny, N., Tudhope, A. W., Webster, J., Westphal, H. and Yokoyama, Y.: Assessing subsidence rates and paleo water-depths for Tahiti reefs using U-Th chronology of altered corals, Mar. Geol., 295–298, 86–94, doi:10.1016/j.margeo.2011.12.006, 2012.

Vaks, A., Woodhead, J., Bar-matthews, M., Ayalon, A., Cliff, R. A. and Zilberman, T.: Pliocene – Pleistocene climate of the northern margin of Saharan – Arabian Desert recorded in speleothems from the Negev Desert, Israel, Earth Planet. Sci. Lett., 368, 88–100, doi:10.1016/j.epsl.2013.02.027, 2013a.

Vaks, A., Gutareva, O. S., Breitenbach, S. F. M., Avirmed, E., Mason, A. J., Thomas, A. L., Osinzev, A. V, Kononov, A. M. and Henderson, G. M.: Speleothems reveal 500,000-year history of Siberian permafrost., Science (80-.)., 61(21), 183–186 [online] Available from: http://www.ncbi.nlm.nih.gov/pubmed/23429705, 2013b.

Vaks, A., Mason, A. J., Breitenbach, S. F. M., Kononov, A. M., Osinzev, A. V., Rosensaft, M., Borshevsky, A., Gutareva, O. S. and Henderson, G. M.: Palaeoclimate evidence of vulnerable permafrost during times of low sea ice, Nature, 577(7789), 221–225, doi:10.1038/s41586-019-1880-1, 2020.

Wang, Z. S., Rasbury, E. T., Hanson, G. N. and Meyers, W. J.: Using the U-Pb system of calcretes to date the time of sedimentation of clastic sedimentary rocks, Geochim. Cosmochim. Acta, 62(16), 2823–2835, doi:https://doi.org/10.1016/S0016-7037(98)00201-4, 1998.

Weyer, S., Anbar, A. D., Gerdes, A., Gordon, G. W., Algeo, T. J. and Boyle, E. A.: Natural fractionation of ^{238}U/^{235}U, Geochim. Cosmochim. Acta, 72(2), 345–359, doi:10.1016/j.gca.2007.11.012, 2008.

Woodhead, J. and Petrus, J.: Exploring the advantages and limitations of in situ U–Pb carbonate geochronology using speleothems, Geochronology, 1(1), 69–84, doi:10.5194/gchron-1-69-2019, 2019.

Woodhead, J. and Pickering, R.: Beyond 500 ka : Progress and prospects in the U \ Pb chronology of speleothems, and their application to studies in palaeoclimate , human evolution, biodiversity and tectonics, Chem. Geol., 322–323, 290–299, doi:10.1016/j.chemgeo.2012.06.017, 2012.

Woodhead, J., Hellstrom, J., Maas, R., Drysdale, R., Zanchetta, G., Devine, P. and Taylor, E.: U – Pb geochronology of speleothems by MC-ICPMS, Quat. Geochronol., 1, 208–221, doi:10.1016/j.quageo.2006.08.002, 2006.

York, D.: Least squares fitting of a straight line with correlated errors, Earth Planet. Sci. Lett., 5(Xi), 320–324, 1969.